

Short-range constraints on chemical and structural variations in bavenite

A. J. LUSSIER AND F. C. HAWTHORNE*

Department of Geological Sciences, University of Manitoba, Winnipeg, Manitoba, Canada R3T 2N2

[Received 30 November 2010; Accepted 30 January 2011]

ABSTRACT

Bavenite is an orthorhombic calcium beryllium aluminosilicate, $a \approx 23.2$, $b \approx 5.0$, $c \approx 19.4$ Å, $V \approx 2250$ Å³, $Z = 4$, that crystallizes in the space group *Cmcm*. The crystal structures of 24 bavenite samples from various localities worldwide were refined to R_1 values from 2.4 to 7.5% based on ~1330 unique reflections collected with Mo- $K\alpha$ X-radiation on a Bruker P4 CCD single-crystal diffractometer. The composition of each crystal was determined by electron microprobe analysis. There is extensive solid-solution in bavenite according to ${}^{O(2)}\text{OH}^- + {}^{T(4)}\text{Si}^{4+} + {}^{T(3)}\text{Be}^{2+} \rightleftharpoons {}^{O(2)}\text{O}^{2-} + {}^{T(4)}\text{Al}^{3+} + {}^{T(3)}\text{Si}^{4+}$, such that the general formula may be written $\text{Ca}_4\text{Be}_x\text{Si}_9\text{Al}_{4-x}\text{O}_{28-x}(\text{OH})_x$, where x ranges from 2.00 to ~3.00 a.p.f.u. Small amounts of additional Be may be incorporated into bavenite *via* the substitution ${}^{T(3)}\text{Be} + {}^{O(2)}\text{OH}^- + \text{Na} + {}^{T(4)}\text{Si}_2 \rightleftharpoons {}^{T(3)}\text{Si} + {}^{O(2)}\text{O}^{2-} + \text{Ca} + {}^{T(4)}\text{Al}_2$. Local (short-range) bond-valence considerations indicate that Short-Range Order (SRO) should be extensive in the bavenite structure, and this is confirmed by Fourier Transform Infrared (FTIR) spectroscopy in the principal OH-stretching region and by ${}^{27}\text{Al}$ Magic Angle Spinning Nuclear Magnetic Resonance (MAS NMR) spectroscopy. Short-range bond-valence considerations indicate that the $T(3)$ – $T(4)$ – $T(3)$ – $T(4)$ rings of the framework can incorporate any short-range arrangement of cations consonant with their site populations [$T(3) = \text{Be, Si}$; $T(4) = \text{Si, Al}$], and ${}^{27}\text{Al}$ MAS NMR spectroscopy confirms this, showing the presence of the local clusters ${}^{T(3)}\text{Be}$ – ${}^{T(4)}\text{Al}$ – ${}^{T(3)}\text{Be}$, ${}^{T(3)}\text{Si}$ – ${}^{T(4)}\text{Al}$ – ${}^{T(3)}\text{Be}$ and ${}^{T(3)}\text{Si}$ – ${}^{T(4)}\text{Al}$ – ${}^{T(3)}\text{Si}$. Incorporation of Be at the $T(3)$ site is accompanied by local replacement of O^{2-} by $(\text{OH})^-$ at the O(2) site and hydrogen bonding to the adjacent O(3) anion; the latter promotes $\text{Be} \rightarrow \text{Si}$ substitution at the $T(3)$ tetrahedron adjacent in the **b** direction. $T(3)$ – $T(4)$ – $T(3)$ – $T(4)$ rings link in the **c** direction through a $T(3)$ –(1)–(3) linkage [$T(1) = \text{Si}$]. Local bond-valence considerations show that occupancy of both $T(3)$ tetrahedra by Be violates the valence-sum rule, and that the linkage ${}^{T(3)}\text{Be}$ – ${}^{T(1)}\text{Si}$ – ${}^{T(3)}\text{Si}$ provides the constraint whereby Be does not exceed 3 a.p.f.u. in bavenite when incorporated *via* the substitution ${}^{O(2)}\text{OH}^- + {}^{T(4)}\text{Si}^{4+} + {}^{T(3)}\text{Be}^{2+} \rightleftharpoons {}^{O(2)}\text{O}^{2-} + {}^{T(4)}\text{Al}^{3+} + {}^{T(3)}\text{Si}^{4+}$.

KEYWORDS: Bavenite, crystal-structure refinement, IR, ${}^{27}\text{Al}$ MAS NMR, EMPA, beryllium, end-members, solid-solution.

Introduction

BAVENITE is a calcium beryllium aluminosilicate mineral occurring primarily in granitic pegmatites (Černý, 2002). It is a widespread product of

hydrothermal alteration, particularly of beryl (Černý, 1968; Bondi *et al.*, 1983), and can occur as pseudomorphs after beryl. It also occurs as coatings on feldspar and quartz in miarolitic pegmatites (Tennyson, 1960; Janeczek, 1985). Bavenite has been reported from pneumatolytically altered syenites (Petersen *et al.*, 1995), where it is definitely not pseudomorphic, occurring as large (up to 1.5 cm) freestanding crystals on albite. The first detailed chemical compositions were given by Switzer and Reichen (1960),

* E-mail: frank_hawthorne@umanitoba.ca
DOI: 10.1180/minmag.2011.075.1.213

Berry (1963), Beus (1966) and Cannillo *et al.* (1966), and both Cannillo *et al.* (1966) and Kharitonov *et al.* (1971) showed that the crystal structure is a framework of silicate and beryllate tetrahedra with the formula $\text{Ca}_4 [\text{Be}_{(2+x)}\text{Al}_{(2-x)}] [\text{Si}_9\text{O}_{(26-x)}(\text{OH})_{(2+x)}]$. Different substitution mechanisms have been proposed to account for the variation in chemical composition of bavenite. Berry (1963) suggested $\text{Be} \rightleftharpoons \text{Al}$ with electroneutrality maintained by the incorporation of H. Cannillo *et al.* (1966) solved the structure of bavenite; they assigned Be and Al to the *T*(2) and *T*(4) tetrahedra, and proposed that additional minor Be replaces Al at the *T*(4) site. In addition, IR spectra were reported by Petersen *et al.* (1995).

In the present study, we have characterized the crystal structure and crystal chemistry of 24 samples of bavenite (Table 1) using single-

crystal X-ray diffraction (XRD), IR spectroscopy and electron microprobe analysis (EMPA) in order to examine the details of the substitution mechanism, the role of hydrogen bonding in the structure, and the character of short-range order associated with the solid solution. Several other samples were also characterized by crystal-structure refinement and EMPA, and show disorder that is not present in the samples described here; these results will be reported at a later date.

Experimental

X-ray diffraction

Crystals were selected for study based on optical clarity and uniform extinction in cross-polarized light. Each fragment was attached to the end of a

TABLE 1. List of bavenite samples and locations of origin.

	Locality	Other number	Source
2ABAV	Rincon, San Diego County, California	118245-B	b
7BAV	Ilimaussaq, Kangerluarsuk Fjord, Greenland	134693	b
10BAV	Government Pit, Albany, New Hampshire	119542	b
11BAV	Kalisay, Kyrgyzstan	—	a
12BAV	Baveno, Italy	E3365	c
13BAV	Londonderry, West Australia	M23357	c
14BAV	Sandvik Property, Zealand Twp., Kenora District, Ontario	M405225	c
15BAV	Foote Mine, King's Mountain, Cleavland County, North Carolina	teach113	c
19BAV	Lily Pad Lake, Fort Hope, Ontario, Canada	M38292	c
21BAV	Aple Rossa, Oresco, Novara, Italy	M41009	c
23BAV	Oresco, Val Vigeddo, Italy	—	d
25BAV	Ascham Alm, Untersulzbachtal, Salzburg, Austria	—	e
27BAV	Lily Pad Lake, Fort Hope, Ontario, Canada	M6128	f
28BAV	Lily Pad Lake, Fort Hope, Ontario, Canada	M5617	f
29BAV	Lily Pad Lake, Fort Hope, Ontario, Canada	M5617	f
31BAV	Drahonin A, Czech Republic	a 122	g
32BAV	Marsikov, Schinderhubel 1, Czech Republic	a 1380	g
33BAV	Vlastejovice, Czech Republic	B 5963	g
35BAV	Mont Saint-Hilaire, Quebec, Canada	—	j
36BAV	Nye Rull, Buskerud, Norway	—	i
37BAV	Baveno, Italy	—	i
39BAV	Norway	—	i
40BAV	Lily Pad Lake, Fort Hope, Ontario, Canada	—	k
41BAV	Ekaterinburg (near), Ural, Russia	—	k

a: Excaliber Mineral Co.; b: Harvard University; c: Royal Ontario Museum; d: Dealer; e: Natural History Museum, Vienna; f: Petr Černý; g: Moravia Museum of Mineralogy; h: Geologisk Museum, Copenhagen; i: Roy Kristiansen; j: Andy McDonald; k: Chris Pedersen.

tapered glass fibre and mounted on a Bruker *P4* automated four-circle X-ray diffractometer equipped with a graphite monochromated Mo- $K\alpha$ X-radiation and a Bruker 4K CCD detector. X-ray intensity data were collected to $60^\circ 2\theta$ with a frame width of 0.2° and frame times from 40 to 120 s to ensure equal data coverage for crystals of different size. Unit-cell dimensions were derived for each crystal by least-squares refinement of ~ 1720 unique reflections in the Ewald sphere; values are given in Table 2, together with other information relevant to data collection and structure refinement. The data were corrected for absorption, Lorentz, polarization and background effects, averaged and reduced to structure factors.

Chemical composition

Crystals were analysed using a Cameca SX-100 electron microprobe operating in wavelength-dispersion mode with an accelerating voltage of 15 kV, a specimen current of 15 nA, and a beam diameter of 10 μm . The following standards were used: TAP: Al, andalusite; Si, diopside; LTAP: Mg, olivine; LLiF: Mn, spessartine; Fe, fayalite; Na, albite; LPET: K, orthoclase; Ca, diopside. Unit formulae were normalized on the basis of 28 anions with $\text{Be} = 13 - (\text{Si} + \text{Al})$ a.p.f.u. (atoms per formula unit) and OH was iterated until $(\text{Ca} + \text{Na}) = (\text{Al} + \text{Be})$. Chemical compositions (mean of 10 determinations) and unit formulae are given in Table 3.

Crystal-structure refinement

The structure of each sample was refined in the space group *Cmcm* using F^2 in the *SHELXTL PLUS* (PC version) software package; initial positional parameters were those of Cannillo *et al.* (1966). Full occupancy was assumed for all sites, and there was no subsequent indication of vacancies. The *T*(3) site is occupied by Si and Be, and the site occupancies were allowed to vary during refinement, subject to the constraint that $\text{Si} + \text{Be} = 1$. The position of the H atom associated with the O(8) O atom was taken from difference-Fourier maps and refined with a fixed isotropic-displacement parameter and fixed occupancy. The constraint of electroneutrality indicates that some crystals have H present in addition to that attached to O(8). Bond-valence calculations showed that this additional H is attached to the O atom at the O(2) site, but the exact position of this H could not

be seen on difference-Fourier maps, perhaps because of local disorder associated with variations in short-range bond-valence values (see later discussion). An extinction correction was introduced in the final stages of refinement, and all structures converged to R_1 indices in the range 2.3–7.5%, although the majority (20 structures) are in the range 2.3–4.5%. Final atom coordinates and isotropic-displacement parameters are given in Table 4; anisotropic-displacement parameters for all structures have been deposited with the editor of the journal and are available at http://www.minersoc.org/pages/e_journals/dep_mat_mm.html. Selected interatomic distances are given in Table 5, refined site-scattering values (Hawthorne *et al.*, 1995) are given in Table 6 (where they are compared with the values from the unit formulae derived from chemical compositions determined by EMPA), and Table 7 shows selected bond-valence tables calculated with the parameters of Brown and Altermatt (1985).

Fourier-transform infrared spectroscopy (FTIR)

A Bruker Tensor 27 Fourier-transform infrared (FTIR) spectrometer equipped with an MCT detector was used to collect spectra on five powdered samples of bavenite (25BAV, 32BAV, 35BAV, 40BAV and 41BAV). For 25BAV and 35BAV, we collected X-ray powder patterns to check for impurity phases, but none was found; there was insufficient material to do so for the other samples. Approximately 5 mg of ground mineral was combined with 145 mg of ground KBr and pressed into a single pellet under 10 tons of pressure for 20–30 min. All pellets were thoroughly dried in a heated desiccator at $\sim 106^\circ\text{C}$ for 8–10 h to ensure minimal adsorption of water. For each spectrum, a total of 1000 scans was collected between 4000 and 600 cm^{-1} at a resolution of 4 cm^{-1} and a beam size of 6 mm. Spectra were analysed by fitting symmetric-Gaussian peaks and an asymmetric-Gaussian background with the software package *PeakFit*[®] (v.4) by optimization and least-squares refinement until an acceptable fit to the spectral shape was obtained.

Magic-Angle-Spinning Nuclear Magnetic Resonance (MAS NMR) spectroscopy

A Varian Inova 600 spectrometer (14.1 T) was used to record MAS NMR spectra of ^{27}Al ($\nu_L = 156.3\text{ MHz}$) for 40BAV and 41BAV. For each

TABLE 2. Data collection and structure-refinement information for bavenite samples.

	2ABAV	7BAV	10BAV	11BAV	12BAV	13BAV	14BAV	15BAV
a (Å)	23.2080(10)	23.2028(6)	23.2068(14)	23.2110(10)	23.198(2)	23.2164(10)	23.2066(9)	23.1995(11)
b (Å)	4.9833(2)	4.9805(1)	4.9929(3)	4.9721(2)	4.9620(4)	5.0023(2)	4.9681(2)	5.0111(2)
c (Å)	19.4266(8)	19.4290(5)	19.4340(12)	19.4189(7)	19.4262(14)	19.4447(7)	19.4085(8)	19.4454(9)
V (Å ³)	2246.7(3)	2245.2(2)	2251.7(4)	2241.1(3)	2236.1(5)	2258.2(3)	2237.7(3)	2260.6(3)
R_1	2.95	2.33	3.34	2.77	4.50	3.10	3.03	2.92
wR_2	8.14	6.83	8.41	7.54	9.78	8.66	8.11	7.28
GoF	1.036	1.074	1.032	1.077	0.890	1.093	1.002	1.001
Reflections collected	10670	10610	10761	10706	10649	10741	10524	10733
Reflections merged	1709	1713	1726	1708	1709	1726	1709	1732
$\Sigma F_o > 4\sigma F$	1306	1491	1291	1358	968	1497	1315	1277
$R_{\text{int ORTH}}$	4.9	3.0	6.0	3.9	13.8	3.4	5.0	5.8
Crystal dimensions (μm)	$50 \times 50 \times 240$	$80 \times 100 \times 120$	$140 \times 200 \times 3$	$180 \times 100 \times 40$	$100 \times 200 \times 2$	$120 \times 240 \times 30$	$60 \times 160 \times 25$	$120 \times 200 \times 10$
	19BAV	21BAV	23BAV	25BAV	27BAV	28BAV	29BAV	31BAV
a (Å)	23.2075(8)	23.2077(12)	23.197(3)	23.2120(7)	23.2090(7)	23.2074(7)	23.2066(7)	23.2096(14)
b (Å)	5.0063(2)	5.0096(2)	4.9847(5)	5.0043(1)	5.0129(1)	5.0098(2)	4.9960(2)	5.0020(3)
c (Å)	19.4428(7)	19.4422(8)	19.416(2)	19.4439(6)	19.4494(6)	19.4477(7)	19.4373(7)	19.4386(10)
V (Å ³)	2258.9(2)	2260.4(3)	2245.2(7)	2258.6(2)	2262.8(2)	2261.1(2)	2253.6(2)	2256.7(4)
R_1	2.52	3.02	5.72	2.51	2.35	2.49	2.34	3.60
wR_2	7.29	7.08	10.81	7.12	7.02	6.71	7.01	9.02
GoF	1.123	0.960	0.889	1.101	1.062	1.052	1.130	1.047
Reflections collected	10619	10780	10625	10750	10705	10754	10702	10664
Reflections merged	1729	1726	1708	1727	1724	1731	1724	1721
$\Sigma F_o > 4\sigma F$	1428	1235	856	1516	1494	1366	1433	1353
$R_{\text{int ORTH}}$	4.0	6.5	20.1	3.0	3.2	4.3	3.2	5.6
Crystal dimensions (μm)	$60 \times 100 \times 160$	$110 \times 130 \times 16$	$140 \times 25 \times 13$	$80 \times 80 \times 180$	$70 \times 140 \times 160$	$80 \times 80 \times 100$	$80 \times 80 \times 200$	$100 \times 140 \times 20$

Table 2 (contd.)

	32BAV	33BAV	35BAV	36ABAV	37BAV	39BAV	40BAV	41BAV
a (Å)	23.1995(12)	23.1949(11)	23.251(2)	23.2043(11)	23.2272(6)	23.2051(11)	23.1895(12)	23.1961(13)
b (Å)	4.9743(3)	5.0067(2)	4.9734(5)	5.0005(5)	5.0028(1)	4.9986(2)	4.9725(2)	4.9937(3)
c (Å)	19.4255(9)	19.4370(8)	19.4678(14)	19.4426(9)	19.4518(5)	19.4375(9)	19.4488(9)	19.4296(11)
V (Å ³)	2241.7(3)	2257.2(3)	2251.2(6)	2255.98(18)	2260.3(2)	2254.6(3)	2242.62(17)	2250.6(2)
R_1	3.43	3.06	7.28	5.08	3.22	3.22	3.74	7.45
wR_2	8.46	8.33	16.21	10.04	7.52	7.98	8.95	13.76
GoF	1.071	1.028	1.024	1.316	1.157	1.082	1.127	1.404
Σ Reflections collected	10626	10694	10583	11092	10565	10525	10945	10976
Σ Reflections merged	1710	1724	1714	1719	1719	1719	1715	1725
$\Sigma F_o > 4\sigma F$	1367	1399	1082	1729	1447	1338	1649	1715
R_{int}^{ORTH}	5.6	4.4	16.6	2.9	3.9	5.0	2.9	3.5
Crystal dimensions (μ m)	40 × 80 × 140	30 × 130 × 220	100 × 100 × 4	100 × 160 × 40	140 × 80 × 38	100 × 180 × 15	20 × 50 × 50	60 × 60 × 150

sample, weighed amounts (10–35 mg) of powdered sample (~15 μ m crystallites) were placed in a 3.2 mm (22 μ L capacity) zirconia rotor and spun at a speed of 18 kHz (41BAV) and 22 kHz (40BAV) in a double-resonance probe. An optimized recycle delay of 60 s was used for both samples, as this was determined to be more than sufficient to ensure complete relaxation. The final spectra are composites of 1024 averaged scans. Spectra are referenced to 1.1 M Al(NO₃)₃. Pulse widths were selected to coincide approximately with a 20° tip angle at an rf nutation frequency of 50 kHz. The ²⁷Al spectra for bavenite lack well defined lineshapes required to obtain NMR parameters by simulation. For both spectra, component peaks were sufficiently resolved to allow reliable modelling using symmetric Lorentzian-Gaussian peakshapes, from which the integrated intensities for each peak could be determined.

General structure description

Bavenite has a framework structure of silicate and beryllate tetrahedra (Cannillo *et al.*, 1966). Four-membered rings of alternating SiO₄ and AlO₄ tetrahedra link through six-membered rings of SiO₄ tetrahedra to form chains that extend in the **a** direction (Fig. 1a). Adjacent chains link through linear BeO₄–SiO₄–BeO₄ groups, forming two types of six-membered rings between the chains: [^{T(2)}Be–^{T(1)}Si–^{T(3)}(Si, Be)–^{T(4)}(Al, Si)–^{T(5)}Si–^{T(6)}Si] and [^{T(2)}Be–^{T(6)}Si–^{T(6)}Si–^{T(2)}Be–^{T(6)}Si–^{T(6)}Si] (Fig. 1b). These sheets stack in the **b** direction (Fig. 2), with AlO₄ tetrahedra as the linking elements between the sheets. This arrangement results in large cavities that contain the [7]-coordinated interstitial Ca.

In the bavenite structure, the ratio of the number of tetrahedral cations and anions is 13:28, indicating that the framework is interrupted (i.e. all anions do not link to two *T* cations). For a completely continuous framework structure, the ideal formula is [*T*Φ₂]_n where Φ is an unspecified anion. A completely connected framework of tetrahedra with thirteen cations would have the formula [*T*₁₃Φ₂₆], and hence the formula [*T*₁₃Φ₂₈] must have four [1]-coordinated anions. These are the O(2) and O(8) anions, both of which occur twice in the formula unit [*T*₁₃Φ₂₈]. Bond-valence considerations (see below) show that O(8) is always an (OH) group, and O(2) may be O or (OH), depending on the details of the short-range coordination.

Results

Site populations

Crystal-structure refinement indicates that variation in site-scattering values occurs only at the $T(3)$ site (Table 6). In addition, there is significant variation in $\langle T-O \rangle$ bondlengths at the $T(3)$ and $T(4)$ sites. The $\langle T-O \rangle$ bondlengths at $T(1)$, $T(2)$, $T(5)$ and $T(6)$ show little variation: $\langle T(1)-O \rangle = 1.636(2)$, $\langle T(2)-O \rangle = 1.646(2)$, $\langle T(5)-O \rangle = 1.620(4)$, $\langle T(6)-O \rangle = 1.618(1)$ Å. The variation in $\langle T(1)-O \rangle$, $\langle T(5)-O \rangle$ and $\langle T(6)-O \rangle$, 1.618–1.636 Å, is in accord with the variation in mean anion coordination number ([4], [2.5] and [2.25], respectively) for SiO_4 tetrahedra (Brown and Gibbs, 1969), and hence we assign $T(1) = T(5) = T(6) = \text{Si}$. Site-scattering indicates that $T(2)$ is occupied by Be, as found by Cannillo *et al.*

(1966). The $\langle T(2)-O \rangle$ distance of 1.646(2) Å is somewhat longer than the grand $\langle \text{Be}-O \rangle$ distance in minerals of 1.633 Å reported by Hawthorne and Huminicki (2002), but still lies well within the dispersion of their data, and the low scatter in bavenite indicates that $T(2)$ is completely occupied by Be as proposed by Cannillo *et al.* (1966). Thus, the principal variation at the T sites involves (1) variation in site scattering at $T(3)$, and (2) variation in $\langle T-O \rangle$ at $T(4)$.

Variation in site scattering at $T(3)$ is accompanied by little or no change in the $\langle T(3)-O \rangle$ bondlength (~ 1.625 Å), which is in accord with occupancy of $T(3)$ by Be and Si (with radii of 0.27 and 0.26 Å, respectively, Shannon, 1976). Figure 3 shows the variation in Be calculated from the chemical compositions of the crystals

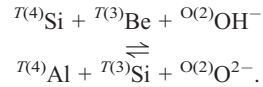
TABLE 3. EMPA-derived composition of single crystals.

		2ABAV	7BAV	10BAV	11BAV	12BAV	13BAV	14BAV	15BAV	19BAV	21BAV	23BAV	25BAV
Na_2O		0.17	0.08	0.13	0.02	0.30	0.12	0.09	0.03	0.0	0.01	0.04	0.05
Al_2O_3		6.57	8.23	7.74	5.87	3.54	8.23	5.17	10.30	9.5	9.99	7.30	9.60
SiO_2		59.15	59.35	59.41	58.82	61.48	58.34	59.37	57.67	59.0	58.13	59.03	58.22
CaO		24.14	23.95	24.26	24.79	23.44	23.89	24.49	24.39	24.3	24.41	24.51	24.25
BaO		7.68	6.71	7.12	8.19	8.96	6.71	8.46	5.85	6.2	5.99	7.38	6.15
H_2O		2.83	2.50	2.62	2.91	3.48	2.46	3.07	2.06	2.2	2.13	2.66	2.21
Total		100.54	100.82	101.28	100.60	101.20	99.76	100.64	100.29	101.3	100.66	100.92	100.47
$Ca:$	Na	0.050	0.024	0.037	0.006	0.087	0.036	0.026	0.009	0.003	0.003	0.012	0.015
	Ca	3.940	3.917	3.946	4.042	3.745	3.953	3.977	4.050	3.976	4.033	3.999	4.007
	Σ	3.990	3.941	3.983	4.048	3.832	3.989	4.003	4.060	3.979	4.036	4.011	4.022
$T(1):$	Si	1.000	1.000	1.000	1.000	1.000	1.000	1.000	1.000	1.000	1.000	1.000	1.000
$T(2):$	Be	2.000	2.000	2.000	2.000	2.000	2.000	2.000	2.000	2.000	2.000	2.000	2.000
$T(3):$	Si	1.189	1.540	1.402	1.005	0.790	1.510	0.920	1.822	1.740	1.780	1.299	1.723
	Be	0.811	0.460	0.598	0.995	1.210	0.490	1.080	0.178	0.260	0.220	0.701	0.277
	Σ	2.000	2.000	2.000	2.000	2.000	2.000	2.000	2.000	2.000	2.000	2.000	2.000
$T(2):$	Si	0.821	0.519	0.615	0.947	1.378	0.501	1.077	0.118	0.282	0.184	0.690	0.255
	Al	1.179	1.481	1.385	1.053	0.622	1.499	0.923	1.882	1.718	1.816	1.310	1.745
	Σ	2.000	2.000	2.000	2.000	2.000	2.000	2.000	2.000	2.000	2.000	2.000	2.000
$T(5):$	Si	2.000	2.000	2.000	2.000	2.000	2.000	2.000	2.000	2.000	2.000	2.000	2.000
$T(6):$	Si	4.000	4.000	4.000	4.000	4.000	4.000	4.000	4.000	4.000	4.000	4.000	4.000
$O(1)-O(7):$	O	24.000	24.000	24.000	24.000	24.000	24.000	24.000	24.000	24.000	24.000	24.000	24.000
$O(8):$	OH	2.000	2.000	2.000	2.000	2.000	2.000	2.000	2.000	2.000	2.000	2.000	2.000
$O(2):$	O	1.129	1.457	1.348	1.047	0.535	1.463	0.897	1.872	1.715	1.813	1.298	1.730
	OH	0.871	0.543	0.652	0.953	1.465	0.537	1.103	0.128	0.285	0.187	0.702	0.270
	Σ	2.000	2.000	2.000	2.000	2.000	2.000	2.000	2.000	2.000	2.000	2.000	2.000

CHEMICAL AND STRUCTURAL VARIATIONS IN BAVENITE

determined by EMPA (Table 3) as a function of the Be content of the $T(3)$ site determined by SREF (Hawthorne and Grice, 1990). The data scatter about the 1:1 line, but there is a tendency to lie slightly below the 1:1 line; however, using ionized scattering factors moves the data to slightly above the line. The general accord between the SREF and EMPA results indicates that both methods of deriving the Be content are reasonably accurate, and that variable Be occurs only at the $T(3)$ site. There is no significant variation in scattering at the $T(4)$ site and yet there is significant variation in the $\langle T(4)-O \rangle$ distances (Table 5) from 1.653–1.730 Å. This variation in $\langle T(4)-O \rangle$ and lack of variation in site scattering is compatible with occupancy of $T(4)$ by Si ($Z = 14$, $r = 0.26$ Å) and Al ($Z = 13$, $r = 0.39$ Å). In accord with this conclusion, there is a linear

relation between $\langle T(4)-O \rangle$ and the Al content of the crystal (Fig. 4). Figure 5 shows the variation of Al at the $T(4)$ site as a function of Be at the $T(3)$ site. This inverse 1:1 relation is in exact accord with the substitution



Hydrogen bonding

Inspection of the bond-valence tables (Table 7) for crystals 14BAV (high Be) and 27BAV (low Be) shows that, omitting hydrogen bonds, two anions have incident bond-valence sums significantly less than the value of 2 v.u. (valence units) expected from the valence-sum rule (Brown,

Table 3 (contd.)

		27BAV	28BAV	29BAV	31BAV	32BAV	33BAV	35BAV	36ABAV	37BAV	39BAV	40BAV	41BAV
Na ₂ O		0.04	0.02	0.03	0.07	0.05	0.03	0.50	0.06	0.09	0.06	0.10	0.05
Al ₂ O ₃		9.79	10.32	6.12	8.83	6.19	9.08	3.36	9.19	7.78	7.50	5.65	8.19
SiO ₂		58.10	58.54	59.45	58.47	59.42	57.69	60.80	58.97	58.85	58.81	59.03	57.88
CaO		23.43	24.39	24.38	24.33	24.48	24.16	23.84	24.01	24.10	24.44	23.97	23.95
BaO		5.68	5.83	7.90	6.58	7.92	6.35	9.39	6.25	7.00	7.27	8.00	6.70
H ₂ O		2.12	2.09	2.88	2.37	2.88	2.26	3.58	2.31	2.57	2.62	2.95	2.43
Total		99.16	101.19	100.75	100.64	100.93	99.57	101.47	100.78	100.39	100.70	99.70	99.20
Ca:	Na	0.012	0.006	0.009	0.022	0.014	0.010	0.145	0.018	0.027	0.018	0.030	0.015
	Ca	3.919	4.010	3.966	4.002	3.977	4.024	3.803	3.943	3.956	4.000	3.932	3.989
	Σ	3.931	4.016	3.975	4.024	3.990	4.034	3.948	3.961	3.983	4.018	3.962	4.004
$T(1)$	Si	1.000	1.000	1.000	1.000	1.000	1.000	1.000	1.000	1.000	1.000	1.000	1.000
$T(2)$	Be	2.000	2.000	2.000	2.000	2.000	2.000	2.000	2.000	2.000	2.000	2.000	2.000
$T(3)$	Si	1.870	1.850	1.120	1.573	1.115	1.630	0.642	1.699	1.422	1.333	1.058	1.497
	Be	0.130	0.150	0.880	0.427	0.885	0.370	1.358	0.301	0.578	0.667	0.942	0.503
	Σ	2.000	2.000	2.000	2.000	2.000	2.000	2.000	2.000	2.000	2.000	2.000	2.000
$T(2)$	Si	0.199	0.133	0.905	0.403	0.895	0.336	1.410	0.340	0.595	0.649	0.980	0.500
	Al	1.801	1.867	1.095	1.597	1.105	1.664	0.590	1.660	1.405	1.351	1.020	1.500
	Σ	2.000	2.000	2.000	2.000	2.000	2.000	2.000	2.000	2.000	2.000	2.000	2.000
$T(5)$	Si	2.000	2.000	2.000	2.000	2.000	2.000	2.000	2.000	2.000	2.000	2.000	2.000
$T(6)$	Si	4.000	4.000	4.000	4.000	4.000	4.000	4.000	4.000	4.000	4.000	4.000	4.000
O(1)–O(7): O		24.000	24.000	24.000	24.000	24.000	24.000	24.000	24.000	24.000	24.000	24.000	24.000
O(8): OH		2.000	2.000	2.000	2.000	2.000	2.000	2.000	2.000	2.000	2.000	2.000	2.000
O(2): O		1.789	1.861	1.086	1.575	1.092	1.654	0.445	1.642	1.378	1.333	0.990	1.485
	OH	0.211	0.139	0.914	0.425	0.908	0.346	1.555	0.358	0.622	0.667	1.010	0.515
	Σ	2.000	2.000	2.000	2.000	2.000	2.000	2.000	2.000	2.000	2.000	2.000	2.000

TABLE 4. Final atom positions and equivalent isotropic-displacement parameters (\AA^2) for crystals of bavenite.

		2ABAV	7BAV	10BAV	11BAV	12BAV	13BAV	14BAV	15BAV
<i>Ca</i>	<i>x</i>	0.08316(2)	0.08264(1)	0.08343(2)	0.08246(2)	0.08175(4)	0.08358(2)	0.08246(2)	0.08409(2)
	<i>y</i>	0.25083(10)	0.25225(7)	0.24779(10)	0.25168(9)	0.2578(2)	0.24639(8)	0.25474(10)	0.24341(9)
	<i>z</i>	0.15316(3)	0.15336(2)	0.15288(3)	0.15327(2)	0.15418(4)	0.15279(2)	0.15347(2)	0.15245(3)
	U_{eq}	0.01349(13)	0.01283(10)	0.01301(14)	0.01355(12)	0.0142(2)	0.01325(13)	0.01302(13)	0.01013(12)
<i>T(1)</i>	<i>x</i>	0	0	0	0	0	0	0	0
	<i>y</i>	0.7762(3)	0.77468(17)	0.7773(3)	0.772(2)	0.7725(5)	0.7774(2)	0.7742(3)	0.7795(3)
	<i>z</i>	1/4	1/4	1/4	1/4	1/4	1/4	1/4	1/4
	U_{eq}	0.0086(3)	0.00850(17)	0.0088(3)	0.0095(2)	0.0081(5)	0.0093(2)	0.0079(3)	0.0067(3)
<i>T(2)</i>	<i>x</i>	0.12460(18)	0.12434(13)	0.1248(2)	0.12424(17)	0.1241(3)	0.12475(16)	0.12439(18)	0.1249(2)
	<i>y</i>	0.8188(9)	0.8213(6)	0.8179(9)	0.8211(8)	0.8235(16)	0.8158(8)	0.8223(9)	0.8140(9)
	<i>z</i>	1/4	1/4	1/4	1/4	1/4	1/4	1/4	1/4
	U_{eq}	0.0074(8)	0.0106(5)	0.0092(9)	0.0118(8)	0.0100(17)	0.0097(7)	0.0092(8)	0.0091(9)
<i>T(3)</i>	<i>x</i>	0	0	0	0	0	0	0	0
	<i>y</i>	0.7224(3)	0.72113(18)	0.7228(2)	0.7203(3)	0.7216(6)	0.72300(19)	0.7220(3)	0.72322(19)
	<i>z</i>	0.10362(7)	0.10437(5)	0.10419(7)	0.10458(6)	0.10338(14)	0.10435(5)	0.10354(8)	0.10442(5)
	U_{eq}	0.0083(4)	0.0087(3)	0.0080(4)	0.0094(4)	0.0084(9)	0.0098(3)	0.0087(5)	0.0066(3)
<i>T(4)</i>	<i>x</i>	0.09415(4)	0.09400(3)	0.09465(5)	0.09372(4)	0.09309(7)	0.09492(4)	0.09334(4)	0.09567(4)
	<i>y</i>	1/2	1/2	1/2	1/2	1/2	1/2	1/2	1/2
	<i>z</i>	0	0	0	0	0	0	0	0
	U_{eq}	0.0065(3)	0.0071(2)	0.0078(3)	0.0081(3)	0.0076(5)	0.0087(3)	0.0066(3)	0.0069(3)
<i>T(5)</i>	<i>x</i>	0.17025(4)	0.17025(3)	0.17020(4)	0.17005(3)	0.17006(7)	0.17026(3)	0.16995(4)	0.17033(4)
	<i>y</i>	0	0	0	0	0	0	0	0
	<i>z</i>	0	0	0	0	0	0	0	0
	U_{eq}	0.0099(2)	0.00960(14)	0.0098(2)	0.01049(18)	0.0089(3)	0.01000(18)	0.0095(2)	0.0079(2)
<i>T(6)</i>	<i>x</i>	0.21413(3)	0.21395(2)	0.21404(3)	0.21387(2)	0.21372(5)	0.21409(2)	0.21395(3)	0.21415(3)
	<i>y</i>	0.85950(13)	0.86185(8)	0.85830(14)	0.86129(12)	0.8670(2)	0.85757(11)	0.86276(13)	0.85491(13)
	<i>z</i>	0.14428(3)	0.14400(2)	0.14362(4)	0.14392(3)	0.14452(5)	0.14342(3)	0.14434(3)	0.14311(3)
	U_{eq}	0.00859(15)	0.00858(11)	0.00903(16)	0.00951(13)	0.0081(2)	0.00931(14)	0.00823(15)	0.00740(15)
<i>O(1)</i>	<i>x</i>	0	0	0	0	0	0	0	0
	<i>y</i>	0.5757(5)	0.5746(3)	0.5758(5)	0.5717(4)	0.5756(8)	0.5754(4)	0.5748(5)	0.5757(4)
	<i>z</i>	0.18208(12)	0.18229(8)	0.18238(13)	0.18225(10)	0.18213(19)	0.18265(10)	0.18191(11)	0.18288(12)
	U_{eq}	0.0098(5)	0.0099(3)	0.0105(5)	0.0107(4)	0.0094(9)	0.0105(4)	0.0097(5)	0.0088(5)
<i>O(2)</i>	<i>x</i>	0	0	0	0	0	0	0	0
	<i>y</i>	0.0366(5)	0.0364(3)	0.0360(5)	0.0337(4)	0.0370(8)	0.0363(4)	0.0363(5)	0.0362(5)
	<i>z</i>	0.11016(13)	0.10970(9)	0.11158(14)	0.11071(10)	0.1082(2)	0.11202(12)	0.10896(12)	0.11344(12)
	U_{eq}	0.0127(5)	0.0129(3)	0.0129(6)	0.0114(4)	0.013(1)	0.0137(4)	0.0112(5)	0.0103(5)
<i>O(3)</i>	<i>x</i>	0.05747(7)	0.05766(5)	0.05771(8)	0.05783(6)	0.05742(12)	0.05767(7)	0.05747(7)	0.05763(7)
	<i>y</i>	0.5972(3)	0.5957(2)	0.5981(4)	0.5961(3)	0.5933(6)	0.5980(3)	0.5953(4)	0.5997(3)
	<i>z</i>	0.06905(9)	0.06957(6)	0.07017(10)	0.06979(7)	0.06836(14)	0.07061(8)	0.06855(8)	0.07143(9)
	U_{eq}	0.0144(4)	0.0147(3)	0.0140(4)	0.0151(3)	0.0124(6)	0.0151(3)	0.0145(4)	0.0118(4)
<i>O(4)</i>	<i>x</i>	0.13055(7)	0.13101(5)	0.13117(8)	0.13110(7)	0.13069(12)	0.13135(7)	0.13050(7)	0.13163(7)
	<i>y</i>	0.2394(3)	0.2369(2)	0.2345(4)	0.2367(3)	0.2410(6)	0.2328(3)	0.2412(4)	0.2302(3)
	<i>z</i>	0.03389(10)	0.03407(6)	0.03488(10)	0.03410(8)	0.03210(13)	0.03539(8)	0.03336(9)	0.03624(9)
	U_{eq}	0.0143(4)	0.0145(3)	0.0143(4)	0.0157(3)	0.0141(7)	0.0144(3)	0.0146(4)	0.0114(4)

CHEMICAL AND STRUCTURAL VARIATIONS IN BAVENITE

Table 4 (contd.)

		2ABAV	7BAV	10BAV	11BAV	12BAV	13BAV	14BAV	15BAV
O(5)	x	0.20832(7)	0.20826(5)	0.20825(8)	0.20806(6)	0.20770(12)	0.20829(6)	0.20823(7)	0.20832(7)
	y	0.8702(4)	0.8718(2)	0.8683(4)	0.8723(3)	0.8777(7)	0.8669(3)	0.8738(4)	0.8638(3)
	z	0.06111(9)	0.06072(6)	0.06049(9)	0.06065(7)	0.06124(13)	0.06028(8)	0.06105(8)	0.05984(8)
	U_{eq}	0.0139(4)	0.0139(2)	0.0140(4)	0.0145(3)	0.0125(6)	0.0141(3)	0.0134(4)	0.0118(4)
O(6)	x	0.23315(8)	0.23320(5)	0.23340(8)	0.23296(7)	0.23307(12)	0.23342(7)	0.23308(7)	0.23368(7)
	y	0.5583(3)	0.5603(2)	0.5581(4)	0.5585(3)	0.5642(5)	0.5575(3)	0.5603(3)	0.5556(3)
	z	0.16618(9)	0.16554(6)	0.16530(9)	0.16527(7)	0.16577(13)	0.16511(8)	0.16616(8)	0.16476(9)
	U_{eq}	0.0115(4)	0.0120(2)	0.0119(4)	0.0125(3)	0.0106(7)	0.0130(3)	0.0112(3)	0.0097(4)
O(7)	x	0.15428(7)	0.15437(5)	0.15449(8)	0.15439(6)	0.15426(12)	0.15456(7)	0.15415(7)	0.15462(7)
	y	0.9349(3)	0.9381(2)	0.9320(4)	0.9376(3)	0.9430(6)	0.9317(3)	0.9397(3)	0.9287(3)
	z	0.18009(9)	0.18009(6)	0.18001(10)	0.17999(7)	0.18014(14)	0.18005(8)	0.18013(8)	0.17986(9)
	U_{eq}	0.0121(4)	0.0126(2)	0.0121(4)	0.0128(3)	0.0113(6)	0.0133(3)	0.0116(4)	0.0103(4)
O(8)	x	0.12108(10)	0.12121(7)	0.12110(11)	0.12121(9)	0.12103(17)	0.12100(9)	0.12117(9)	0.12102(11)
	y	0.4919(5)	0.4935(3)	0.4900(5)	0.4917(4)	0.4975(8)	0.4903(4)	0.4947(5)	0.4879(5)
	z	¼	¼	¼	¼	¼	¼	¼	¼
	U_{eq}	0.0113(5)	0.0116(3)	0.0121(6)	0.0127(4)	0.0114(9)	0.0127(4)	0.0106(5)	0.0108(5)
O(9)	x	0.05802(10)	0.05806(7)	0.05832(11)	0.05795(8)	0.05789(16)	0.05849(9)	0.05786(9)	0.05862(10)
	y	0.9555(4)	0.9560(3)	0.9538(5)	0.9553(4)	0.9593(8)	0.9537(4)	0.9574(5)	0.9523(4)
	z	¼	¼	¼	¼	¼	¼	¼	¼
	U_{eq}	0.0087(5)	0.0093(3)	0.0094(5)	0.0105(4)	0.0082(9)	0.0106(4)	0.0088(5)	0.0083(5)
H(8)	x	0.1627(3)	0.1619(4)	0.1627(3)	0.1626(3)	0.1606(9)	0.1620(4)	0.1622(4)	0.1626(3)
	y	0.459(8)	0.441(6)	0.4572(8)	0.452(7)	0.428(11)	0.442(7)	0.448(8)	0.454(7)
	z	¼	¼	¼	¼	¼	¼	¼	¼
	U_{eq}	0.015*	0.015*	0.015*	0.015*	0.015*	0.015*	0.015*	0.015*
		19BAV	21BAV	23BAV	25BAV	27BAV	28BAV	29BAV	31BAV
Ca	x	0.08394(2)	0.08389(2)	0.08300(5)	0.08388(1)	0.08411(1)	0.08398(2)	0.08358(2)	0.08362(2)
	y	0.24425(7)	0.24434(11)	0.2506(2)	0.24491(7)	0.24308(6)	0.24394(8)	0.24703(7)	0.24636(11)
	z	0.15255(2)	0.15255(3)	0.15317(5)	0.15264(2)	0.15241(2)	0.15248(2)	0.15280(2)	0.15276(3)
	U_{eq}	0.01119(11)	0.01062(12)	0.0119(3)	0.01245(10)	0.01111(10)	0.01172(11)	0.01269(11)	0.01103(14)
T(1)	x	0	0	0	0	0	0	0	0
	y	0.7782(2)	0.7782(3)	0.7756(6)	0.77755(18)	0.77933(17)	0.7785(2)	0.77710(19)	0.7779(3)
	z	¼	¼	¼	¼	¼	¼	¼	¼
	U_{eq}	0.0077(2)	0.0075(3)	0.0077(6)	0.00868(18)	0.00781(18)	0.0083(2)	0.00829(19)	0.0068(3)
T(2)	x	0.12516(15)	0.1250(2)	0.1251(4)	0.12506(12)	0.12519(13)	0.12505(16)	0.12482(14)	0.12497(19)
	y	0.8141(7)	0.814(1)	0.8196(17)	0.8139(6)	0.8137(6)	0.8136(7)	0.8159(7)	0.816(1)
	z	¼	¼	¼	¼	¼	¼	¼	¼
	U_{eq}	0.0086(6)	0.009(1)	0.005(2)	0.0094(5)	0.0096(5)	0.0098(7)	0.0093(6)	0.0072(9)
T(3)	x	0	0	0	0	0	0	0	0
	y	0.72302(16)	0.7230(2)	0.7212(6)	0.72270(15)	0.72297(13)	0.72301(17)	0.72305(17)	0.7229(2)
	z	0.10442(4)	0.10446(5)	0.10402(14)	0.10440(4)	0.10453(4)	0.10448(4)	0.10413(4)	0.10423(6)
	U_{eq}	0.0075(2)	0.006(3)	0.007(1)	0.0087(2)	0.0078(2)	0.0083(3)	0.0088(3)	0.0068(4)
T(4)	x	0.09529(4)	0.09546(5)	0.09423(10)	0.09497(3)	0.09553(3)	0.09541(4)	0.09471(3)	0.09494(5)
	y	½	½	½	½	½	½	½	½
	z	0	0	0	0	0	0	0	0
	U_{eq}	0.0071(2)	0.0070(3)	0.0067(8)	0.0085(2)	0.0077(2)	0.0081(3)	0.0075(2)	0.0065(3)

Table 4 (contd.)

		19BAV	21BAV	23BAV	25BAV	27BAV	28BAV	29BAV	31BAV
T(5)	x	0.17028(3)	0.17025(4)	0.17016(10)	0.17021(3)	0.17034(3)	0.17026(3)	0.17021(3)	0.17020(4)
	y	0	0	0	0	0	0	0	0
	z	0	0	0	0	0	0	0	0
	U_{eq}	0.00872(16)	0.0085(2)	0.0098(5)	0.00974(14)	0.00878(14)	0.00938(17)	0.00968(15)	0.0080(2)
T(6)	x	0.21415(2)	0.21412(3)	0.21386(7)	0.21413(2)	0.21415(2)	0.21413(2)	0.21409(2)	0.21410(3)
	y	0.85518(10)	0.85569(14)	0.8603(3)	0.85570(9)	0.85448(9)	0.85503(11)	0.85745(10)	0.85725(14)
	z	0.14322(3)	0.14323(3)	0.14393(7)	0.14332(2)	0.14301(2)	0.14315(3)	0.14361(2)	0.14345(3)
	U_{eq}	0.00814(13)	0.00785(15)	0.0083(3)	0.00903(11)	0.00838(11)	0.00878(13)	0.00865(12)	0.00717(16)
O(1)	x	0	0	0	0	0	0	0	0
	y	0.5750(4)	0.5758(5)	0.5755(9)	0.5751(3)	0.5751(3)	0.5755(4)	0.5750(4)	0.5754(5)
	z	0.18271(9)	0.18297(11)	0.1831(3)	0.18258(9)	0.18274(8)	0.18293(10)	0.18243(9)	0.18264(12)
	U_{eq}	0.0099(4)	0.0089(5)	0.0092(12)	0.0106(3)	0.0099(3)	0.0100(4)	0.0103(4)	0.0085(5)
O(2)	x	0	0	0	0	0	0	0	0
	y	0.0350(4)	0.0363(5)	0.0382(9)	0.0346(4)	0.0354(3)	0.0354(4)	0.0355(4)	0.0359(5)
	z	0.11309(10)	0.11309(12)	0.1108(3)	0.11255(9)	0.11354(9)	0.11329(11)	0.11164(10)	0.11197(13)
	U_{eq}	0.0118(4)	0.0111(5)	0.0129(13)	0.0136(3)	0.0119(3)	0.0127(4)	0.0126(4)	0.0108(5)
O(3)	x	0.05752(6)	0.05764(8)	0.05737(16)	0.05739(5)	0.05761(5)	0.05763(6)	0.05747(5)	0.05752(8)
	y	0.5995(3)	0.5991(3)	0.5942(7)	0.5988(2)	0.5998(2)	0.5998(3)	0.5982(3)	0.5988(4)
	z	0.07113(7)	0.07132(8)	0.06987(18)	0.07101(7)	0.07149(7)	0.07138(8)	0.07027(7)	0.07061(9)
	U_{eq}	0.0136(3)	0.0123(4)	0.0112(9)	0.0152(3)	0.0137(3)	0.0140(3)	0.0148(3)	0.0126(4)
O(4)	x	0.13125(6)	0.13157(7)	0.13128(15)	0.13109(6)	0.13148(5)	0.13145(6)	0.13104(6)	0.13131(8)
	y	0.2317(3)	0.2307(4)	0.2360(7)	0.2325(2)	0.2302(2)	0.2311(3)	0.2348(3)	0.2333(4)
	z	0.03601(7)	0.03596(9)	0.03429(17)	0.03575(7)	0.03639(6)	0.03606(8)	0.03515(7)	0.03538(10)
	U_{eq}	0.0131(3)	0.0118(4)	0.0128(8)	0.0141(3)	0.0123(3)	0.0131(3)	0.0140(3)	0.0126(4)
O(5)	x	0.20830(6)	0.20836(8)	0.20816(16)	0.20829(5)	0.20829(5)	0.20825(6)	0.20829(5)	0.20825(7)
	y	0.8648(3)	0.8644(4)	0.8698(7)	0.8655(2)	0.8640(2)	0.8642(3)	0.8673(3)	0.8663(4)
	z	0.06005(7)	0.06003(8)	0.06059(17)	0.06025(6)	0.05992(6)	0.05994(7)	0.06048(6)	0.06026(9)
	U_{eq}	0.0125(3)	0.0124(4)	0.0126(8)	0.0138(3)	0.0127(2)	0.0132(3)	0.0138(3)	0.0122(4)
O(6)	x	0.23353(6)	0.23378(8)	0.23354(15)	0.23343(5)	0.23361(5)	0.23358(6)	0.23337(5)	0.23336(8)
	y	0.5551(3)	0.5563(3)	0.5601(6)	0.5556(2)	0.5549(2)	0.5556(3)	0.5573(3)	0.5572(4)
	z	0.16495(7)	0.16470(8)	0.16556(18)	0.16518(6)	0.16479(6)	0.16475(7)	0.16539(6)	0.16516(9)
	U_{eq}	0.0111(3)	0.0102(4)	0.0109(9)	0.0125(3)	0.0116(2)	0.0115(3)	0.0119(3)	0.0104(4)
O(7)	x	0.15456(6)	0.15469(7)	0.15479(15)	0.15456(5)	0.15464(5)	0.15463(6)	0.15439(5)	0.15452(8)
	y	0.9298(3)	0.9292(4)	0.9346(7)	0.9307(2)	0.9288(2)	0.9291(3)	0.9324(3)	0.9314(4)
	z	0.17998(7)	0.17972(8)	0.17973(18)	0.18002(6)	0.18000(6)	0.17986(7)	0.18002(7)	0.17988(9)
	U_{eq}	0.0112(3)	0.0111(4)	0.0107(8)	0.0127(3)	0.0119(3)	0.0120(3)	0.0123(3)	0.0103(4)
O(8)	x	0.12113(8)	0.12100(11)	0.1205(2)	0.12116(7)	0.12104(7)	0.12109(8)	0.12114(7)	0.12093(11)
	y	0.4883(4)	0.4885(5)	0.492(1)	0.4884(3)	0.4877(3)	0.4879(4)	0.4897(4)	0.4900(5)
	z	$\frac{1}{4}$	$\frac{1}{4}$	$\frac{1}{4}$	$\frac{1}{4}$	$\frac{1}{4}$	$\frac{1}{4}$	$\frac{1}{4}$	$\frac{1}{4}$
	U_{eq}	0.0112(4)	0.0115(5)	0.0094(11)	0.0122(3)	0.0118(3)	0.0123(4)	0.0119(4)	0.0102(5)
O(9)	x	0.05864(8)	0.05853(11)	0.0585(2)	0.05854(7)	0.05876(7)	0.05870(8)	0.05842(7)	0.05851(10)
	y	0.9528(4)	0.9526(5)	0.955(1)	0.9529(3)	0.9523(3)	0.9523(4)	0.9540(4)	0.9533(5)
	z	$\frac{1}{4}$	$\frac{1}{4}$	$\frac{1}{4}$	$\frac{1}{4}$	$\frac{1}{4}$	$\frac{1}{4}$	$\frac{1}{4}$	$\frac{1}{4}$
	U_{eq}	0.0095(4)	0.0091(5)	0.0102(12)	0.0102(3)	0.0095(3)	0.0101(4)	0.0097(3)	0.0086(5)
H(8)	x	0.1629(2)	0.1625(3)	0.1601(11)	0.1624(3)	0.1626(2)	0.1624(3)	0.1625(3)	0.1627(3)
	y	0.461(6)	0.453(8)	0.424(13)	0.4458(9)	0.453(6)	0.448(7)	0.44942(11)	0.463(9)
	z	$\frac{1}{4}$	$\frac{1}{4}$	$\frac{1}{4}$	$\frac{1}{4}$	$\frac{1}{4}$	$\frac{1}{4}$	$\frac{1}{4}$	$\frac{1}{4}$
	U_{eq}	0.015*	0.015*	0.015*	0.015*	0.015*	0.015*	0.015*	0.015*

CHEMICAL AND STRUCTURAL VARIATIONS IN BAVENITE

Table 4 (contd.)

		32BAV	33BAV	35BAV	36ABAV	37BAV	39BAV	40BAV	41BAV
Ca	x	0.08269(2)	0.08406(2)	0.08173(5)	0.08377(3)	0.08346(2)	0.08366(2)	0.08215(2)	0.08367(4)
	y	0.25323(11)	0.24351(9)	0.2584(3)	0.24583(14)	0.24646(10)	0.2466(10)	0.25394(11)	0.2462(2)
	z	0.15349(3)	0.15246(2)	0.15440(6)	0.15279(3)	0.15288(2)	0.15275(3)	0.15377(3)	0.15286(5)
	U _{eq}	0.01248(13)	0.01240(13)	0.0127(3)	0.01111(16)	0.01205(12)	0.01178(13)	0.01369(13)	0.0108(2)
T(1)	x	0	0	0	0	0	0	0	0
	y	0.7748(3)	0.7790(2)	0.7744(7)	0.7784(4)	0.7775(3)	0.7779(3)	0.7721(3)	0.7773(6)
	z	¼	¼	¼	¼	¼	¼	¼	¼
	U _{eq}	0.0074(3)	0.0091(2)	0.0065(6)	0.0069(3)	0.0077(2)	0.0079(3)	0.0090(3)	0.0071(5)
T(2)	x	0.12453(19)	0.12507(17)	0.1242(5)	0.1248(2)	0.12486(17)	0.12468(18)	0.12437(17)	0.1250(4)
	y	0.8206(9)	0.8133(8)	0.828(2)	0.8151(12)	0.8144(8)	0.8160(9)	0.8208(9)	0.8151(17)
	z	¼	¼	¼	¼	¼	¼	¼	¼
	U _{eq}	0.0090(8)	0.0096(7)	0.010(2)	0.007(1)	0.0087(8)	0.0079(8)	0.0063(7)	0.0061(15)
T(3)	x	0	0	0	0	0	0	0	0
	y	0.7218(3)	0.72308(19)	0.7204(9)	0.7223(3)	0.7229(2)	0.7231(2)	0.7201(2)	0.7211(5)
	z	0.10384(7)	0.10456(5)	0.1030(2)	0.10425(7)	0.10424(5)	0.10413(6)	0.10421(8)	0.10440(12)
	U _{eq}	0.0076(5)	0.0090(3)	0.0105(13)	0.0065(4)	0.0078(3)	0.0075(3)	0.0095(5)	0.0066(7)
T(4)	x	0.09378(4)	0.09524(4)	0.09319(10)	0.09506(6)	0.09493(4)	0.09497(4)	0.09375(4)	0.09468(9)
	y	½	½	½	½	½	½	½	½
	z	0	0	0	0	0	0	0	0
	U _{eq}	0.0065(3)	0.0090(3)	0.0070(7)	0.0068(4)	0.0066(3)	0.0063(3)	0.0070(3)	0.0066(6)
T(5)	x	0.17030(4)	0.17018(4)	0.16995(10)	0.17040(5)	0.17018(4)	0.17032(4)	0.17016(4)	0.17044(8)
	y	0	0	0	0	0	0	0	0
	z	0	0	0	0	0	0	0	0
	U _{eq}	0.0090(2)	0.00998(19)	0.0081(5)	0.0079(2)	0.00810(18)	0.0090(2)	0.00972(19)	0.0079(4)
T(6)	x	0.21400(3)	0.21414(3)	0.21375(7)	0.21418(4)	0.21410(3)	0.21415(3)	0.21392(3)	0.21420(6)
	y	0.86186(14)	0.85474(12)	0.8671(3)	0.85648(18)	0.85831(12)	0.85694(13)	0.86269(13)	0.8562(3)
	z	0.14435(3)	0.14310(3)	0.14453(7)	0.14350(4)	0.14347(3)	0.14362(3)	0.14405(3)	0.14357(7)
	U _{eq}	0.00779(15)	0.00942(14)	0.0067(3)	0.00737(18)	0.00775(14)	0.00777(15)	0.00865(15)	0.0069(3)
O(1)	x	0	0	0	0	0	0	0	0
	y	0.5748(5)	0.5751(4)	0.5745(12)	0.5757(7)	0.5755(5)	0.5755(5)	0.5729(5)	0.5750(10)
	z	0.18221(12)	0.18272(11)	0.1818(3)	0.18264(17)	0.18268(12)	0.18262(12)	0.18240(13)	0.1824(3)
	U _{eq}	0.0094(5)	0.0114(4)	0.0101(12)	0.0097(6)	0.0097(4)	0.0100(5)	0.0113(5)	0.010(1)
O(2)	x	0	0	0	0	0	0	0	0
	y	0.0365(5)	0.0347(5)	0.0359(12)	0.0367(7)	0.0368(5)	0.0371(5)	0.0354(5)	0.0356(10)
	z	0.10951(13)	0.11328(12)	0.1083(3)	0.11201(18)	0.11203(13)	0.11200(13)	0.10949(15)	0.1120(3)
	U _{eq}	0.0119(5)	0.0136(5)	0.0121(13)	0.0115(7)	0.0128(5)	0.0123(5)	0.0145(5)	0.0117(10)
O(3)	x	0.05758(7)	0.05741(7)	0.05761(17)	0.05756(11)	0.05757(7)	0.05757(7)	0.05753(8)	0.05735(16)
	y	0.5959(4)	0.5993(3)	0.5933(9)	0.5985(5)	0.5985(3)	0.5991(3)	0.5955(4)	0.5982(8)
	z	0.06888(9)	0.07145(8)	0.06826(19)	0.07053(13)	0.07051(9)	0.07021(9)	0.06913(10)	0.07057(19)
	U _{eq}	0.0134(4)	0.0149(3)	0.0127(9)	0.0133(5)	0.0135(4)	0.0135(4)	0.0151(4)	0.0136(7)
O(4)	x	0.13074(7)	0.13141(7)	0.13070(17)	0.13117(11)	0.13129(7)	0.13122(7)	0.13086(8)	0.13109(16)
	y	0.2393(4)	0.2309(3)	0.2415(9)	0.2334(5)	0.2331(3)	0.2343(3)	0.2387(4)	0.2339(8)
	z	0.03352(9)	0.03626(8)	0.0323(2)	0.03555(12)	0.03518(9)	0.03513(9)	0.03381(10)	0.03546(18)
	U _{eq}	0.0141(4)	0.0138(3)	0.0131(9)	0.0127(5)	0.0127(3)	0.0130(4)	0.0147(4)	0.0124(7)
O(5)	x	0.20825(7)	0.20825(6)	0.20778(18)	0.20826(10)	0.20816(7)	0.20827(7)	0.20814(8)	0.20812(15)
	y	0.8724(4)	0.8637(3)	0.8789(9)	0.8659(5)	0.8673(3)	0.8660(3)	0.8735(4)	0.8654(8)
	z	0.06123(9)	0.05998(8)	0.06122(18)	0.06041(12)	0.06037(8)	0.06043(9)	0.06087(9)	0.06044(17)
	U _{eq}	0.0137(4)	0.0140(3)	0.0121(9)	0.0123(5)	0.0121(3)	0.0128(4)	0.0139(4)	0.0114(7)

Table 4 (contd.)

		32BAV	33BAV	35BAV	36ABAV	37BAV	39BAV	40BAV	41BAV
O(6)	<i>x</i>	0.23303(8)	0.23346(7)	0.23297(17)	0.23347(10)	0.23366(7)	0.23345(7)	0.23313(8)	0.23336(15)
	<i>y</i>	0.5597(4)	0.5552(3)	0.5654(8)	0.5563(5)	0.5584(3)	0.5568(3)	0.5602(4)	0.5558(7)
	<i>z</i>	0.16607(9)	0.16476(8)	0.16575(19)	0.16528(12)	0.16507(9)	0.16530(9)	0.16560(9)	0.16547(18)
	<i>U</i> _{eq}	0.0110(4)	0.0124(3)	0.0092(9)	0.0109(5)	0.0110(3)	0.0111(4)	0.0123(4)	0.0099(7)
O(7)	<i>x</i>	0.15429(7)	0.15457(7)	0.15418(17)	0.15458(10)	0.15459(7)	0.15446(7)	0.15435(7)	0.15447(15)
	<i>y</i>	0.9380(4)	0.9287(3)	0.9434(8)	0.9314(5)	0.9319(3)	0.93122(3)	0.9394(4)	0.9310(7)
	<i>z</i>	0.18013(9)	0.18000(8)	0.1802(2)	0.18011(12)	0.17991(9)	0.17990(9)	0.18036(9)	0.18009(18)
	<i>U</i> _{eq}	0.0110(4)	0.0127(3)	0.0101(9)	0.0108(5)	0.0113(3)	0.0112(4)	0.0125(4)	0.0100(7)
O(8)	<i>x</i>	0.12109(10)	0.12101(10)	0.1211(2)	0.12101(14)	0.12103(10)	0.12107(10)	0.12132(11)	0.1209(2)
	<i>y</i>	0.4938(5)	0.4881(4)	0.4980(12)	0.4902(7)	0.4898(5)	0.4888(5)	0.4939(5)	0.4898(11)
	<i>z</i>	¼	¼	¼	¼	¼	¼	¼	¼
	<i>U</i> _{eq}	0.0109(5)	0.0128(4)	0.0096(11)	0.0107(6)	0.0116(5)	0.0113(5)	0.0121(5)	0.0101(9)
O(9)	<i>x</i>	0.05811(10)	0.05877(9)	0.0578(2)	0.05859(13)	0.05841(9)	0.05830(10)	0.05801(10)	0.0587(2)
	<i>y</i>	0.9564(5)	0.9524(4)	0.9574(12)	0.9530(7)	0.9532(5)	0.9538(5)	0.9554(5)	0.9525(10)
	<i>z</i>	¼	¼	¼	¼	¼	¼	¼	¼
	<i>U</i> _{eq}	0.0083(5)	0.0099(4)	0.0079(12)	0.0078(6)	0.0092(4)	0.0087(5)	0.0093(5)	0.0072(9)
H(8)	<i>x</i>	0.1625(4)	0.1628(3)	0.1602(15)	0.1601(12)	0.1615(5)	0.1630(2)	0.1617(6)	0.1603(15)
	<i>y</i>	0.4554(7)	0.460(7)	0.425(17)	0.427(12)	0.435(8)	0.466(8)	0.43(1)	0.420(18)
	<i>z</i>	¼	¼	¼	¼	¼	¼	¼	¼
	<i>U</i> _{eq}	0.015*	0.015*	0.015*	0.015*	0.015*	0.015*	0.015*	0.015*

2002): 1.55 and 1.82 v.u. for O(2) and 1.14 and 1.08 v.u. for O(8). These values indicate that the O(8) site is occupied completely by (OH) and the O(2) site is occupied by both (OH) and O²⁻. The position of the H atom associated with the O atom at the O(8) site is shown in detail in Fig. 6. The O–H bond projects out into the cavity between the chains of *T*(6) tetrahedra which extend in the **b** direction (Fig. 6) and there is a hydrogen bond to the O(6) anion that links adjacent *T*(6) tetrahedra.

We were not able to locate the partly occupied H site adjacent to the O(2) anion in difference-Fourier maps in the final stages of refinement. However, space requirements constrain the H atom to lie as indicated in Fig. 7. There are three anions which could possibly act as acceptor anions for a hydrogen bond: O(1), O(3) and O(4). The corresponding anion–anion separations are as follows: O(2)–O(1) ≈ 3.05, O(2)–O(3) ≈ 3.24, O(2)–O(4) ≈ 3.54 Å. All these distances are edges of the *Ca* polyhedron, and hydrogen bonds along the edge of a coordination polyhedron are extremely unusual; however, these are the only possibilities. All distances are reasonable O_{donor}–O_{acceptor} distances for a hydrogen bond, but O(3) as a hydrogen-bond acceptor is more in accord with local bond-valence requirements (see

later discussion). Ideally, the H atom will occur on a mirror plane and will form a bifurcated bond to two symmetry-related O(3) anions. However, the occupancies of the associated symmetry-related pairs of *T*(3) sites and *T*(4) sites do not necessarily obey the long-range symmetry of the structure, and the H(2) atom may be disordered off its special position to form a single hydrogen bond to one of the locally associated O(3) anions.

Chemical composition

As is apparent from Fig. 5, there is extensive solid-solution described by the following exchange: ${}^{T(4)}\text{Si} + {}^{T(3)}\text{Be} + {}^{O(2)}\text{OH}^- \rightleftharpoons {}^{T(4)}\text{Al} + {}^{T(3)}\text{Si} + {}^{O(2)}\text{O}^{2-}$. It is also apparent from this expression that chemical variation in bavenite involves the *T*(3), *T*(4) and O(2) sites, and the remaining sites in the structure have fixed composition (except for minor substitution of Na for Ca at the *Ca* site). Thus we may write the chemical formula of the fixed part of the structure as Ca₄Be₂Si₇O₂₄(OH)₂ and the chemical formula of the variable part of the structure as [(Be,Si)₂(Si,Al)₂(OH,O)₂]. The latter part of the complete formula emphasizes that there are two end-members involved in the bavenite solid-

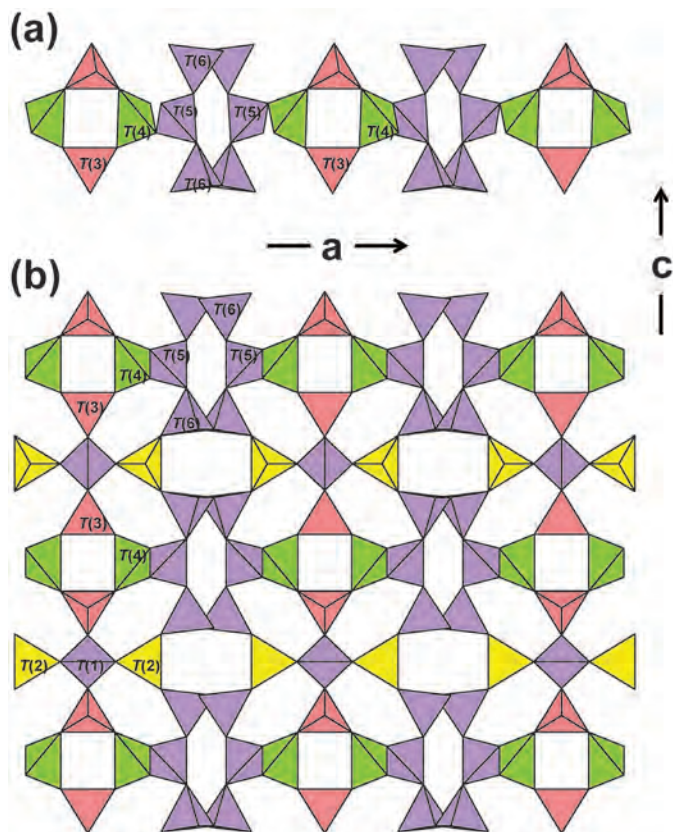


FIG. 1. The crystal structure of bavenite projected down *b*; (a) four-membered rings of $(\text{Si,Be})\text{O}_4$ [$T(3)$, pink] and $(\text{Si,Al})\text{O}_4$ [$T(4)$, green] tetrahedra alternating with six-membered rings of SiO_4 tetrahedra [$T(5)$, $T(6)$, mauve] forming a chain that extends in the *a* direction; (b) chain of Fig. 1a linked in the *c* direction by linear $\text{BeO}_4\text{-SiO}_4\text{-BeO}_4$ [$T(2)$ yellow- $T(1)$ mauve- $T(2)$] trimers.

solution series: $\text{Ca}_4\text{Be}_2\text{Si}_7\text{O}_{24}(\text{OH})_2$ [$\text{Be}_2\text{Si}_2(\text{OH})_2$] and $\text{Ca}_4\text{Be}_2\text{Si}_7\text{O}_{24}(\text{OH})_2$ [$\text{Si}_2\text{Al}_2\text{O}_2$]; this issue is dealt with below. We may also write the general formula of the bavenite solid-solution series as $\text{Ca}_4\text{Be}_2\text{Si}_7\text{O}_{24}(\text{OH})_2$ [(Be,Si) $_2$ (Si,Al) $_2$ (OH,O) $_2$] where the variable part of the formula is written in square brackets.

Beus (1966) wrote the bavenite series as between the compositions $\text{Ca}_4\text{Be}_2\text{Si}_7\text{O}_{24}(\text{OH})_2$ [$\text{BeAlSi}_2(\text{OH})\text{O}$] and $\text{Ca}_4\text{Be}_2\text{Si}_7\text{O}_{24}(\text{OH})_2$ [$\text{Si}_2\text{Al}_2\text{O}_2$]. As is apparent from Fig. 8, the compositions of the current work span this range, but they extend slightly beyond the value of $\text{Be} = 3$ a.p.f.u. to 3.13 a.p.f.u. (from Baveno, Italy) and 3.12 a.p.f.u. (from Mont Saint-Hilaire, Canada); moreover, the former value is supported by the smallest *b* dimension of those recorded here (Fig. 8). However, these two samples are also

characterized by another compositional feature: as shown in Fig. 9, they also have small but significant amounts of Na replacing Ca at the *Ca* site. This suggests that Be may increase past the value of 3 a.p.f.u., but only involving substitution of Na for Ca. It seems that the limit to solid-solution suggested by Beus (1966) is quite strict, and that greater contents of Be can occur only through a different substitution mechanism.

Short-range order in bavenite

The results of crystal-structure refinement give us an average picture of the atomic arrangement in a crystal, and bond-valence arguments generally apply to this average arrangement. However, bond-valence theory also applies to the local structure in a crystal (Hawthorne, 1997) and can

TABLE 5. Selected interatomic distances (Å) in bavenite.

	2ABAV	7BAV	10BAV	11BAV	12BAV	13BAV	14BAV	15BAV	19BAV	21BAV	23BAV	25BAV
Ca—O(1)	2.581(2)	2.563(1)	2.600(2)	2.552(2)	2.525(3)	2.610(1)	2.549(2)	2.632(2)	2.623(1)	2.626(2)	2.582(3)	2.619(1)
Ca—O(2)	2.359(2)	2.356(1)	2.348(2)	2.350(1)	2.365(3)	2.344(1)	2.363(2)	2.337(2)	2.341(1)	2.338(2)	2.346(3)	2.347(1)
Ca—O(3)	2.451(2)	2.431(1)	2.449(2)	2.426(2)	2.423(3)	2.451(2)	2.432(2)	2.459(2)	2.459(1)	2.454(2)	2.429(4)	2.456(1)
Ca—O(4)	2.565(2)	2.576(1)	2.548(2)	2.576(2)	2.631(3)	2.538(2)	2.585(2)	2.515(2)	2.519(1)	2.523(2)	2.567(4)	2.524(1)
Ca—O(7)	2.340(2)	2.343(1)	2.342(2)	2.344(2)	2.350(3)	2.340(2)	2.342(2)	2.334(2)	2.334(1)	2.339(2)	2.350(4)	2.334(1)
Ca—O(8)	2.399(2)	2.402(1)	2.406(2)	2.401(1)	2.390(3)	2.413(1)	2.396(2)	2.415(2)	2.414(1)	2.414(2)	2.395(3)	2.412(1)
Ca—O(9)	2.459(2)	2.455(1)	2.461(2)	2.455(1)	2.442(3)	2.461(1)	2.453(2)	2.465(2)	2.463(1)	2.464(2)	2.455(3)	2.463(1)
<Ca—O>	2.451	2.447	2.451	2.443	2.447	2.451	2.446	2.451	2.450	2.451	2.446	2.451
T(1)—O(1) × 2	1.655(2)	1.650(2)	1.655(3)	1.651(2)	1.641(4)	1.655(2)	1.652(2)	1.657(2)	1.657(2)	1.651(2)	1.637(5)	1.657(2)
T(1)—O(9) × 2	1.616(2)	1.622(2)	1.615(3)	1.624(2)	1.632(4)	1.619(2)	1.622(2)	1.612(2)	1.617(2)	1.615(3)	1.625(5)	1.618(2)
<T(1)—O>	1.636	1.636	1.635	1.637	1.637	1.637	1.637	1.635	1.637	1.633	1.631	1.638
T(2)—O(7) × 2	1.629(3)	1.634(2)	1.629(3)	1.635(3)	1.638(5)	1.632(2)	1.630(3)	1.633(3)	1.629(2)	1.636(3)	1.632(6)	1.632(2)
T(2)—O(8)	1.631(5)	1.634(3)	1.637(5)	1.639(5)	1.620(9)	1.633(4)	1.629(5)	1.636(5)	1.634(4)	1.632(5)	1.641(1)	1.632(3)
T(2)—O(9)	1.688(5)	1.678(3)	1.686(5)	1.677(4)	1.677(8)	1.686(4)	1.684(5)	1.686(5)	1.693(4)	1.692(5)	1.691(1)	1.693(3)
<T(2)—O>	1.644	1.645	1.645	1.647	1.643	1.646	1.643	1.647	1.646	1.649	1.648	1.647
T(3)—O(1)	1.690(3)	1.681(2)	1.688(3)	1.679(2)	1.693(5)	1.692(2)	1.688(3)	1.695(3)	1.693(2)	1.695(3)	1.699(6)	1.690(2)
T(3)—O(2)	1.571(3)	1.574(2)	1.571(3)	1.563(2)	1.568(5)	1.575(2)	1.565(3)	1.578(2)	1.571(2)	1.578(3)	1.586(6)	1.569(2)
T(3)—O(3) × 2	1.618(2)	1.624(1)	1.618(2)	1.625(2)	1.626(3)	1.616(2)	1.624(2)	1.607(2)	1.607(1)	1.609(2)	1.616(4)	1.607(1)
<T(3)—O>	1.624	1.626	1.624	1.623	1.628	1.625	1.625	1.622	1.620	1.623	1.629	1.618
T(4)—O(3) × 2	1.661(2)	1.663(1)	1.684(2)	1.661(2)	1.632(3)	1.696(2)	1.639(2)	1.720(2)	1.712(1)	1.715(2)	1.671(4)	1.706(1)
T(4)—O(4) × 2	1.683(2)	1.701(1)	1.713(2)	1.705(2)	1.674(3)	1.724(2)	1.678(2)	1.738(2)	1.730(1)	1.735(2)	1.707(4)	1.726(1)
<T(4)—O>	1.672	1.682	1.699	1.683	1.653	1.710	1.659	1.729	1.721	1.725	1.689	1.716
T(5)—O(4) × 2	1.645(2)	1.631(1)	1.628(2)	1.625(2)	1.629(3)	1.628(2)	1.641(2)	1.623(2)	1.630(1)	1.622(2)	1.625(4)	1.631(1)
T(5)—O(5) × 2	1.615(2)	1.606(1)	1.611(2)	1.603(2)	1.596(3)	1.611(2)	1.608(2)	1.612(2)	1.612(1)	1.614(2)	1.607(4)	1.615(1)
<T(5)—O>	1.630	1.618	1.620	1.614	1.613	1.620	1.625	1.618	1.621	1.618	1.616	1.623
T(6)—O(5)	1.622(2)	1.624(1)	1.622(2)	1.624(2)	1.625(3)	1.623(2)	1.623(2)	1.625(2)	1.624(1)	1.624(2)	1.624(4)	1.622(1)
T(6)—O(6)	1.621(2)	1.622(1)	1.621(2)	1.623(2)	1.622(3)	1.623(2)	1.623(2)	1.623(2)	1.624(1)	1.622(2)	1.620(3)	1.624(1)
T(6)—O(6)	1.631(2)	1.630(1)	1.631(2)	1.630(2)	1.628(3)	1.632(2)	1.629(2)	1.629(2)	1.629(2)	1.627(2)	1.630(4)	1.632(1)
T(6)—O(7)	1.598(2)	1.596(1)	1.595(2)	1.594(2)	1.589(3)	1.598(2)	1.598(2)	1.599(2)	1.601(1)	1.594(2)	1.581(4)	1.601(1)
<T(6)—O>	1.619	1.618	1.617	1.618	1.616	1.619	1.618	1.619	1.620	1.617	1.614	1.620

CHEMICAL AND STRUCTURAL VARIATIONS IN BAVENITE

	27BAV	28BAV	29BAV	31BAV	32BAV	33BAV	35BAV	36ABAV	37BAV	39BAV	40BAV	41BAV
Ca-O(1)	2.632(1)	2.628(1)	2.603(1)	2.610(2)	2.559(2)	2.628(2)	2.523(4)	2.615(2)	2.608(2)	2.610(2)	2.54(2)	2.606(4)
Ca-O(2)	2.338(1)	2.339(1)	2.349(1)	2.346(2)	2.361(2)	2.340(1)	2.375(3)	2.345(2)	2.343(2)	2.344(2)	2.356(2)	2.346(3)
Ca-O(3)	2.460(1)	2.457(2)	2.453(1)	2.455(2)	2.438(2)	2.457(2)	2.429(4)	2.457(3)	2.456(2)	2.459(2)	2.433(2)	2.453(3)
Ca-O(4)	2.511(1)	2.519(2)	2.539(1)	2.537(2)	2.584(2)	2.512(2)	2.638(4)	2.532(3)	2.546(2)	2.539(2)	2.593(2)	2.533(4)
Ca-O(7)	2.334(1)	2.337(2)	2.335(1)	2.338(2)	2.342(2)	2.334(2)	2.355(4)	2.336(2)	2.341(2)	2.337(2)	2.349(2)	2.336(4)
Ca-O(8)	2.417(1)	2.415(1)	2.408(1)	2.410(2)	2.396(2)	2.414(2)	2.392(4)	2.411(2)	2.411(2)	2.407(2)	2.398(2)	2.406(4)
Ca-O(9)	2.464(1)	2.465(1)	2.460(1)	2.462(2)	2.454(2)	2.462(1)	2.453(4)	2.461(2)	2.462(2)	2.462(2)	2.454(2)	2.46(3)
<Ca-O>	2.451	2.451	2.450	2.451	2.448	2.450	2.452	2.451	2.452	2.451	2.446	2.449
T(1)-O(1)	× 2	1.661(2)	1.657(2)	1.655(3)	1.650(3)	1.659(2)	1.659(6)	1.656(4)	1.654(2)	1.655(2)	1.646(3)	1.657(5)
T(1)-O(9)	× 2	1.616(2)	1.619(2)	1.617(3)	1.623(2)	1.616(2)	1.623(6)	1.616(3)	1.617(2)	1.614(2)	1.625(3)	1.618(5)
<T(1)-O>		1.639	1.638	1.636	1.637	1.638	1.641	1.636	1.636	1.635	1.636	1.638
T(2)-O(7)	× 2	1.629(2)	1.633(3)	1.631(2)	1.631(3)	1.629(3)	1.632(7)	1.632(4)	1.638(3)	1.633(3)	1.633(3)	1.627(6)
T(2)-O(8)		1.637(3)	1.634(4)	1.632(4)	1.634(5)	1.631(4)	1.643(13)	1.627(7)	1.626(5)	1.638(5)	1.627(5)	1.627(10)
T(2)-O(9)		1.691(3)	1.689(4)	1.688(5)	1.683(5)	1.688(4)	1.672(12)	1.684(7)	1.693(5)	1.687(5)	1.678(5)	1.683(10)
<T(2)-O>		1.647	1.646	1.646	1.643	1.644	1.645	1.644	1.649	1.648	1.643	1.641
T(3)-O(1)		1.692(2)	1.695(2)	1.692(2)	1.694(3)	1.690(2)	1.697(7)	1.691(4)	1.695(3)	1.695(3)	1.688(3)	1.681(6)
T(3)-O(2)		1.576(2)	1.574(2)	1.568(2)	1.573(3)	1.570(2)	1.573(7)	1.579(4)	1.578(3)	1.577(3)	1.572(3)	1.578(6)
T(3)-O(3)	× 2	1.607(1)	1.608(1)	1.613(1)	1.611(2)	1.604(2)	1.628(5)	1.612(3)	1.614(2)	1.614(2)	1.621(2)	1.606(4)
<T(3)-O>		1.621	1.621	1.622	1.622	1.617	1.632	1.624	1.625	1.625	1.626	1.618
T(4)-O(3)	× 2	1.720(1)	1.716(2)	1.689(1)	1.698(2)	1.716(2)	1.633(4)	1.697(3)	1.696(2)	1.691(2)	1.655(2)	1.694(4)
T(4)-O(4)	× 2	1.740(1)	1.734(2)	1.713(1)	1.722(2)	1.737(2)	1.676(3)	1.720(3)	1.722(2)	1.714(2)	1.692(2)	1.719(4)
<T(4)-O>		1.730	1.725	1.701	1.710	1.727	1.655	1.709	1.709	1.703	1.674	1.707
T(5)-O(4)	× 2	1.627(1)	1.626(1)	1.634(1)	1.628(2)	1.625(2)	1.634(4)	1.634(3)	1.626(2)	1.632(2)	1.635(2)	1.634(4)
T(5)-O(5)	× 2	1.612(1)	1.612(1)	1.613(1)	1.612(2)	1.614(2)	1.599(4)	1.613(2)	1.612(2)	1.614(2)	1.604(2)	1.611(4)
<T(5)-O>		1.620	1.619	1.624	1.620	1.620	1.617	1.624	1.619	1.623	1.620	1.623
T(6)-O(5)		1.622(1)	1.625(2)	1.622(1)	1.624(2)	1.622(2)	1.629(4)	1.622(3)	1.623(2)	1.623(2)	1.624(2)	1.622(4)
T(6)-O(6)		1.624(1)	1.622(2)	1.621(1)	1.622(2)	1.622(2)	1.619(4)	1.623(3)	1.623(2)	1.622(2)	1.624(2)	1.622(4)
T(6)-O(6)		1.631(1)	1.630(2)	1.632(1)	1.632(1)	1.631(2)	1.637(4)	1.629(3)	1.628(2)	1.629(2)	1.627(2)	1.629(4)
T(6)-O(7)		1.601(1)	1.598(2)	1.600(1)	1.597(2)	1.600(2)	1.595(4)	1.600(2)	1.597(2)	1.598(2)	1.598(2)	1.601(4)
<T(6)-O>		1.620	1.619	1.619	1.619	1.619	1.620	1.619	1.618	1.618	1.618	1.619

TABLE 6. Site-scattering values (e.p.f.u.) for bavenite derived from SREF and EMPA.

	T(3)		T(4)	
	EMPA	SREF	EMPA	SREF
2ABAV	19.9	21.2(2)	26.8	26.0(1)
7BAV	19.2	19.5(1)	26.9	26.7(1)
10BAV	22.0	23.0(2)	26.6	26.1(1)
11BAV	18.0	18.7(1)	26.9	26.7(1)
12BAV	15.0	16.7(2)	27.4	27.0(2)
13BAV	23.1	24.3(2)	26.5	26.3(1)
14BAV	17.2	18.0(2)	27.1	26.1(1)
15BAV	26.2	26.5(1)	26.1	26.3(1)
19BAV	25.4	25.3(1)	26.3	26.3(1)
21BAV	25.8	25.4(2)	26.2	26.4(1)
23BAV	21.0	20.7(3)	26.7	26.3(2)
25BAV	25.2	24.4(1)	26.3	26.4(1)
27BAV	26.7	26.4(1)	26.2	26.3(1)
28BAV	26.5	25.7(1)	26.1	26.3(1)
29BAV	23.4	23.5(1)	26.5	26.1(1)
31BAV	23.7	24.1(2)	26.4	26.1(1)
32BAV	19.1	19.0(2)	26.9	26.9(1)
33BAV	24.3	25.7(1)	26.3	26.2(1)
35BAV	14.4	16.8(4)	27.4	26.9(2)
36ABAV	25.0	24.3(3)	26.3	26.3(2)
37BAV	22.2	24.2(2)	26.6	26.3(1)
39BAV	21.3	24.0(1)	26.6	25.9(1)
40BAV	18.6	18.2(2)	27.0	26.9(1)
41BAV	23.0	23.3(4)	26.5	26.6(3)
<dev.>		0.9		0.3

be used to examine short-range (i.e. non-averaged) arrangements in a structure (Hawthorne *et al.*, 1996a, 2006). Table 7 gives the (average) bond-valence arrangements for a high-Be structure (14BAV) and a low-Be structure (27BAV). We can derive probable bond-valences for ordered arrangements by scaling the bond-valences to sum to the ideal incident sums dictated by the valence-sum rule. Thus for the composition $\text{Ca}_4\text{Be}_2\text{Si}_7\text{O}_{24}(\text{OH})_2[\text{Si}_2\text{Al}_2\text{O}_2]$, we scale the bond valences involving the $T(3)$ and $T(4)$ sites in the low-Be crystal (27BAV) to sum to 4.00 (= Si) and 3.00 v.u. (= Al), respectively, and obtain the bond valences for local (real, not averaged) arrangements of Si and Al that incorporate the effects of strain (at other cations and anions) that are present in the averaged structure (Table 8a). Similarly, for the composition $\text{Ca}_4\text{Be}_2\text{Si}_7\text{O}_{24}(\text{OH})_2[\text{Be}_2\text{Si}_2(\text{OH})_2]$, we scale the bond valences involving the $T(3)$ and $T(4)$ sites in the high-Be crystal (14BAV) to sum to 3.00 (= Be) and 4.00 v.u. (= Si),

respectively (Table 8b). These values may be used for arguments involving short-range order and local structure.

Constraints involving the (OH) anions

The environments of the O(8) and O(2) sites are illustrated in Figs 6 and 7. Excluding H, the O(8) anion is bonded to atoms at the Ca ($\times 2$) and $T(2)$ sites. The $T(2)$ site is occupied only by Be and the Ca site is dominantly occupied by Ca with very minor to trace Na (we will ignore Na in this discussion as it averages 0.02 a.p.f.u. in our samples, except for 35BAV which has 0.145 a.p.f.u. Na). Thus, the nearest-neighbour cations to O(8) will be dominated by Ca and Be: $T(2)\text{Be}-\text{Ca}-\text{Ca}-\text{O}(8)$. The $T(2)$ tetrahedron links only to the $T(6)$ tetrahedron and the Ca polyhedron. As the $T(6)$ site is occupied only by Si, the next-nearest-neighbour sites show no chemical variation and hence no possibilities for different short-range arrangements.

CHEMICAL AND STRUCTURAL VARIATIONS IN BAVENITE

TABLE 7a. Bond-valence calculations for a high-Be (14BAV) bavenite sample.

	Ca	T(1)	T(2)	T(3)	T(4)	T(5)	T(6)	Σ
O(1)	0.21 ^{×2→}	0.93 ^{×2↓}		0.62				1.96
O(2)	0.34 ^{×2→}			0.87				1.55
O(3)	0.28			0.74 ^{×2↓}	0.99 ^{×2↓}			2.01
O(4)	0.19				0.89 ^{×2↓}	0.96 ^{×2↓}		2.04
O(5)						1.04 ^{×2↓}		2.05
O(6)							0.99 ^{×2↓→}	1.98
O(7)	0.36		0.51 ^{×2↓}				1.07	1.95
O(8)	0.31 ^{×2→}		0.51					1.14
O(9)	0.27 ^{×2→}	1.01 ^{×2↓}	0.44					1.98
Σ	1.97	3.87	1.97	2.97	3.78	4.00	4.06	
EMPA	2.00	4.00	2.00	2.92	3.54	4.00	4.00	

Table 7b. Bond valence calculations for a low-Be (27BAV) bavenite sample.

	Ca	T(1)	T(2)	T(3)	T(4)	T(5)	T(6)	Σ
O(1)	0.16 ^{×2→}	0.90 ^{×2↓}		0.81				2.04
O(2)	0.36 ^{×2→}			1.10				1.82
O(3)	0.26			1.01 ^{×2↓}	0.82 ^{×2↓}			2.10
O(4)	0.23				0.78 ^{×2↓}	0.99 ^{×2↓}		2.00
O(5)						1.03 ^{×2↓}		2.04
O(6)							0.99 ^{×2↓→}	1.97
O(7)	0.36		0.51 ^{×2↓}				1.06	1.94
O(8)	0.29 ^{×2→}		0.50					1.08
O(9)	0.26 ^{×2→}	1.02 ^{×2↓}	0.43					1.97
Σ	1.92	3.85	1.96	3.94	3.21	4.05	4.05	
EMPA	1.96	4.00	2.00	3.87	3.10	4.00	4.00	

Excluding H, the O(2) anion is bonded to atoms at the Ca ($\times 2$) and T(3) sites. The T(3) site is occupied by Si and Be and the nearest-neighbour cations will be dominated by Si, Be and Ca; the algebraically possible short-range arrangements are as follows: $T(3)\text{Si}-\text{Ca}-\text{Ca}-\text{O}(2)$ and $T(3)\text{Be}-\text{Ca}-\text{Ca}-\text{O}(2)$. The occupancy of the O(2) site in these local arrangements is controlled by the bond valence incident at the O(2) site. Inspection of Table 8 shows incident bond-valence sums of 2.06 and 1.27 v.u. for the clusters $T(3)\text{Si}-\text{Ca}-\text{Ca}-\text{O}(2)$ and $T(3)\text{Be}-\text{Ca}-\text{Ca}-\text{O}(2)$. Hence the O(2) site is occupied by (OH) where T(3) is locally occupied by Be (Table 8a) and is occupied by O^{2-} where T(3) is locally occupied by Si (Table 8b). Hence there is only one crystal-chemically possible local cluster around the O(2) site where $\text{O}(2) = (\text{OH})$: $T(3)\text{Be}-\text{Ca}-\text{Ca}-\text{O}(2)$.

Possible order involving the T(3)–T(4)–T(3)–T(4) ring

A prominent linkage in the structure of bavenite is the four-membered T(3)–T(4)–T(3)–T(4) ring that may be seen (coloured rose and green) in Fig. 1. The T(3) site may be occupied by Si and Be, and the T(4) site may be occupied by Al and Si. There are nine algebraically possible distinct ring compositions; these are listed in Table 9. The bridging anion in the T(3)–T(4)–T(3)–T(4) ring is O(3); do the bond-valence requirements of the O(3) anion exert any constraints on the possible cation arrangements in the T(3)–T(4)–T(3)–T(4) ring? The O(3) anion is coordinated by the T(3), T(4), Ca and H(2) cations, and the possible local cation arrangements are as follows: $T(3)\text{Be}-T(4)\text{Si}-\text{Ca}-\text{H}(2)$, $T(3)\text{Be}-T(4)\text{Al}-\text{Ca}-\text{H}(2)$, $T(3)\text{Si}-T(4)\text{Al}-\text{Ca}-\text{H}(2)$ and $T(3)\text{Si}-T(4)\text{Si}-\text{Ca}-\text{H}(2)$, where the H(2) site may be occupied

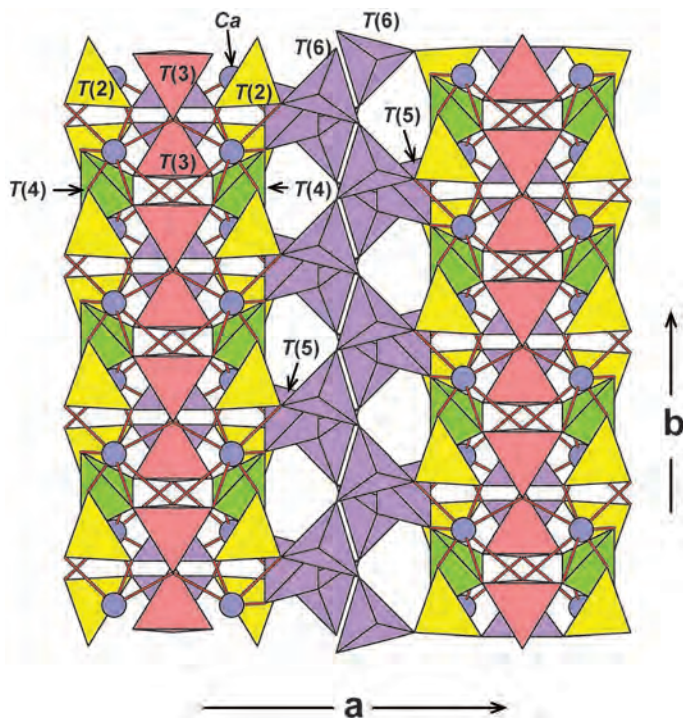


FIG. 2. The crystal structure of bavenite projected onto (001). Legend as in Fig. 1, Ca sites are shown by blue circles, Ca–O bonds are shown by red lines.

by H or \square (vacancy) depending on the local occupancy of the $T(3)$ site in the adjacent $T(3)$ – $T(4)$ – $T(3)$ – $T(4)$ ring. This point is illustrated in Fig. 10. The O(3) anion in the

$T(3)$ – $T(4)$ – $T(3)$ – $T(4)$ ring to the right receives a hydrogen bond from a donor O(2) anion in the adjacent $T(3)$ – $T(4)$ – $T(3)$ – $T(4)$ ring. This is an important point because it means that the arrangements $T^{(3)}\text{Si}$ – $T^{(4)}\text{Al}$ –Ca–H(2) and

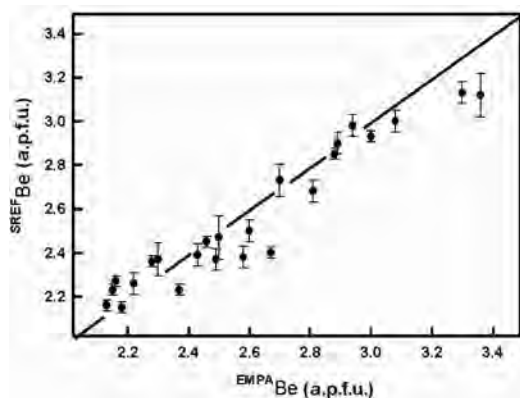


FIG. 3. Variation in Be content derived by SREF as a function of Be content derived by stoichiometric calculation from the electron microprobe analyses (EMPA); the line shows the 1:1 relation.

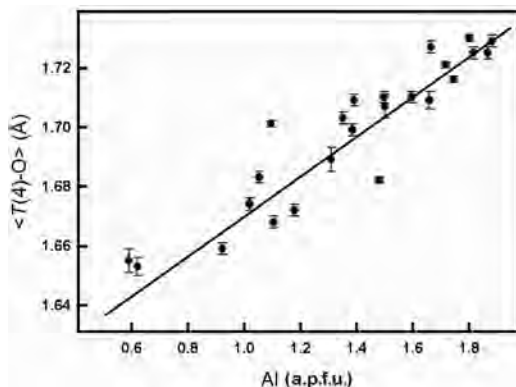


FIG. 4. Variation in $\langle T(4)\text{--}O \rangle$ as a function of Al in bavenite structures; the bars show ± 1 standard deviation.

CHEMICAL AND STRUCTURAL VARIATIONS IN BAVENITE

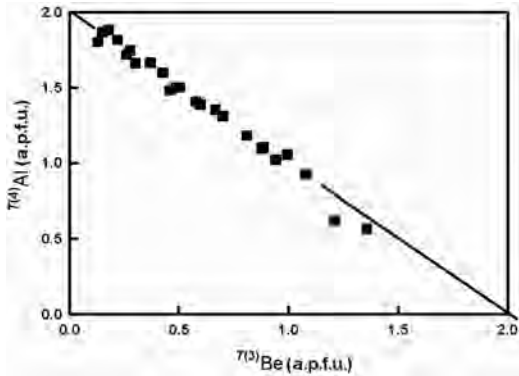


FIG. 5. Variation in $T(4)\text{Al}$ as a function of $T(3)\text{Be}$ in bavenite; the line shows the relation $T(4)\text{Al} + T(3)\text{Be} = 2.0$ a.p.f.u.

$T(3)\text{Si}-T(4)\text{Si}-\text{Ca}-\text{H}(2)$ can have the H(2) site occupied by H (even though the local T(3) site is occupied by Si) because it is the composition of the adjacent ring that affects the occupancy of H(2). From Tables 8a and 8b, the magnitudes of the local bond-valences to O(3) are approximately as follows: $T(3)\text{Be}-\text{O}(3) = 0.50$, $T(3)\text{Si}-\text{O}(3) = 1.03$, $T(4)\text{Si}-\text{O}(3) = 1.05$, $T(4)\text{Al}-\text{O}(3) = 0.77$, $\text{Ca}-\text{O}(3) = 0.27$ and $\text{H}(2) \approx 0.27$ or 0.00 v.u. The bond-valence sums around O(3) for each of these local arrangements are shown in Table 10. These calculations indicate that the arrangements $T(3)\text{Si}-T(4)\text{Si}-\text{Ca}-\text{H}$ (sum = 2.61 v.u.) and

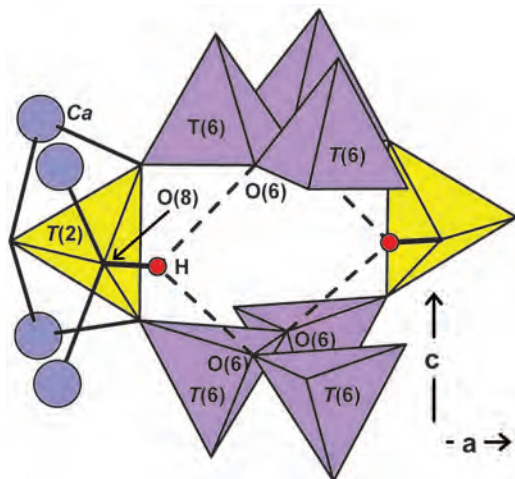


FIG. 6. The hydrogen-bond arrangement around the O(8) anion in bavenite; legend as in Fig. 1, the H atom is shown by a small red circle and hydrogen bonds are shown as black dashed lines.

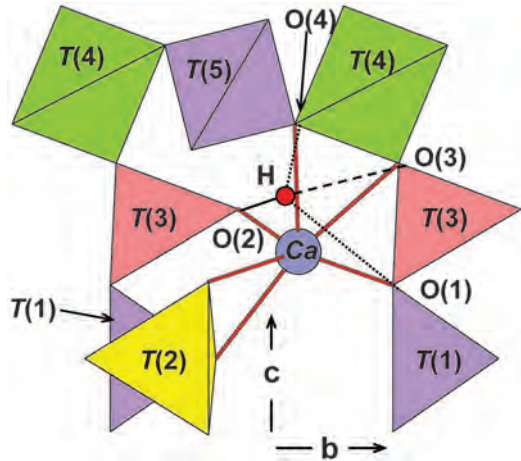


FIG. 7. The hydrogen-bond arrangement around the O(2) anion in bavenite; legend as in Fig. 6, other short O(donor)-O distances are shown by dotted lines.

$T(3)\text{Be}-T(4)\text{Al}-\text{Ca}-\square$ (sum = 1.55 v.u.) cannot occur. The arrangements $T(3)\text{Si}-T(4)\text{Si}-\text{Ca}-\square$ and $T(3)\text{Si}-T(4)\text{Al}-\text{Ca}-\text{H}$ have bond-valence sums of 2.35 v.u., which suggests that these also should not occur. However, the bulk composition of these minerals conforms to the constraint $T(3)\text{Be} = T(4)\text{Si}$. As a result of this, if $T(3)\text{Si}-\text{O}(3)-T(4)\text{Si}$ linkages are not possible, then only $T(3)\text{Be}-\text{O}(3)-T(4)\text{Si}$ and $T(3)\text{Si}-\text{O}(3)-T(4)\text{Al}$ linkages can occur, and there will be no

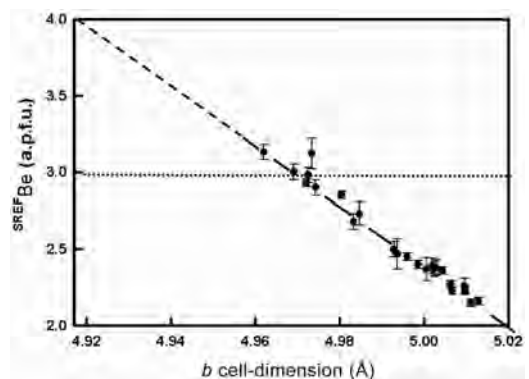


FIG. 8. Variation in SREF Be content as a function of the b cell-dimension in bavenite. The data follow a linear relation (full line) which extrapolates (dashed line) to a Be content of 4 a.p.f.u. at $b \approx 4.918$ Å. The horizontal line shows the maximum extent of the bavenite series proposed by Beus (1966).

TABLE 8a. Bond-valence table for short-range arrangements: $T(3) = \text{Be}$, $T(4) = \text{Si}$.

	Ca	$T(1)$	$T(2)$	$T(3) = \text{Be}$	$T(4) = \text{Si}$	$T(5)$	$T(6)$	Σ	H(2)	H(8)	Σ
O(1)	0.21 $\times 2 \rightarrow$	0.93 $\times 2 \downarrow$		0.41				1.76			1.76
O(2)	0.34 $\times 2 \rightarrow$			0.59				1.27	0.73		2.00
O(3)	0.28			0.50 $\times 2 \downarrow$	1.05 $\times 2 \downarrow$			1.83	0.27		2.10
O(4)	0.19				0.95 $\times 2 \downarrow$	0.96 $\times 2 \downarrow$		2.10			2.10
O(5)						1.04 $\times 2 \downarrow$	1.00	2.04			2.04
O(6)							0.99 $\times 2 \rightarrow$	1.98		0.07	2.05
O(7)	0.36		0.51 $\times 2 \downarrow$				1.07	1.94			1.94
O(8)	0.31 $\times 2 \rightarrow$		0.51					1.13		0.93	2.06
O(9)	0.27 $\times 2 \rightarrow$	1.01 $\times 2 \downarrow$	0.44					1.99			1.99
Σ	1.97	3.87	1.97	2.00	4.00	4.00	4.06		1.00	1.00	

Table 8b. Bond-valence table for short-range arrangements: $T(3) = \text{Si}$, $T(4) = \text{Al}$.

	Ca	$T(1)$	$T(2)$	$T(3) = \text{Si}$	$T(4) = \text{Al}$	$T(5)$	$T(6)$	Σ	H(2)	H(8)	Σ
O(1)	0.16 $\times 2 \rightarrow$	0.90 $\times 2 \downarrow$		0.82				2.04			2.04
O(2)	0.36 $\times 2 \rightarrow$			1.12				1.84			1.84
O(3)	0.26			1.03 $\times 2 \downarrow$	0.77 $\times 2 \downarrow$			2.06			2.06
O(4)	0.23				0.73 $\times 2 \downarrow$	0.99 $\times 2 \downarrow$		1.95			1.95
O(5)						1.03 $\times 2 \downarrow$	1.01	2.04			2.04
O(6)							0.99 $\times 2 \rightarrow$	1.98		0.05	2.03
O(7)	0.36		0.51 $\times 2 \downarrow$				1.06	1.93			1.93
O(8)	0.29 $\times 2 \rightarrow$		0.50					1.08		0.95	2.03
O(9)	0.26 $\times 2 \rightarrow$	1.02 $\times 2 \downarrow$	0.43					1.97			1.97
Σ	1.92	3.85	1.96	4.00	3.00	4.04	4.06			1.00	

$T(3)\text{Be}-\text{O}(3)-T(4)\text{Al}$ linkages. The occurrence of these local arrangements can be tested by ^{27}Al MAS NMR as Al occurs only at $T(4)$ and the resultant band(s) will represent only local environments around the $T(4)$ site. If there are

no $T(3)\text{Si}-\text{O}(3)-T(4)\text{Si}$ linkages, then there is only one local next-nearest-neighbour arrangement involving Al at $T(4)$: $T(3)\text{Si}-T(4)\text{Al}-T(3)\text{Si}$. If there are $T(3)\text{Si}-\text{O}(3)-T(4)\text{Si}$ linkages, then there are three local next-nearest-neighbour arrangements involving Al at $T(4)$: $T(3)\text{Be}-T(4)\text{Al}-T(3)\text{Be}$, $T(3)\text{Si}-T(4)\text{Al}-T(3)\text{Be}$ and $T(3)\text{Si}-T(4)\text{Al}-T(3)\text{Si}$.

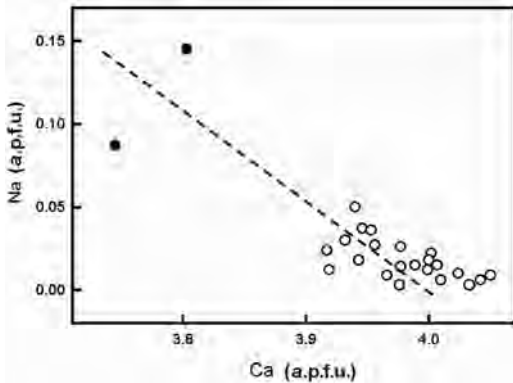


FIG. 9. Variation in Na content as a function of Ca content in bavenite; the black circles denote bavenites with $\text{Be} > 3$ a.p.f.u.

TABLE 9. All possible $T(3)-T(4)-T(3)-T(4)$ configurations.

	$T(3)$	$T(4)$	$T(3)$	$T(4)$
I	Be	Si	Be	Si
II	Be	Si	Be	Al
III	Be	Al	Be	Al
IV	Be	Si	Si	Si
V	Be	Si	Si	Al
VI	Be	Al	Si	Al
VII	Si	Si	Si	Si
VIII	Si	Si	Si	Al
IX	Si	Al	Si	Al

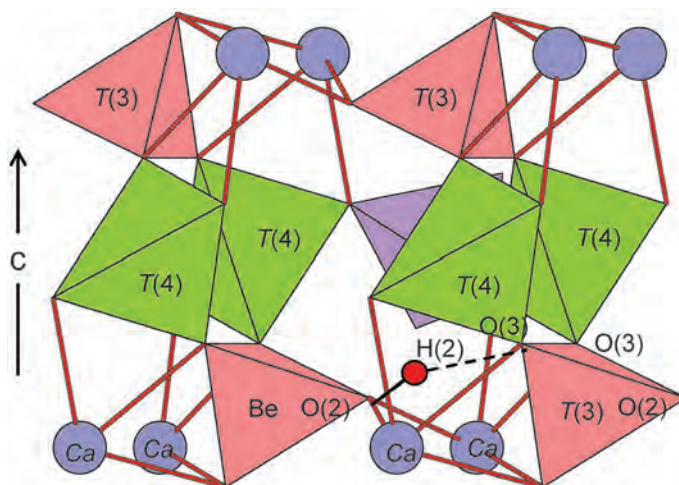


FIG. 10. An oblique view of adjacent $T(3)$ - $T(4)$ - $T(3)$ - $T(4)$ rings in the bavenite structure. The O(3) anion in one ring receives a hydrogen bond from the donor O(2) anion in the adjacent ring. Legend as in Fig. 2.

Figure 11 shows ^{27}Al MAS NMR spectra for samples 40BAV and 41BAV. In each sample,

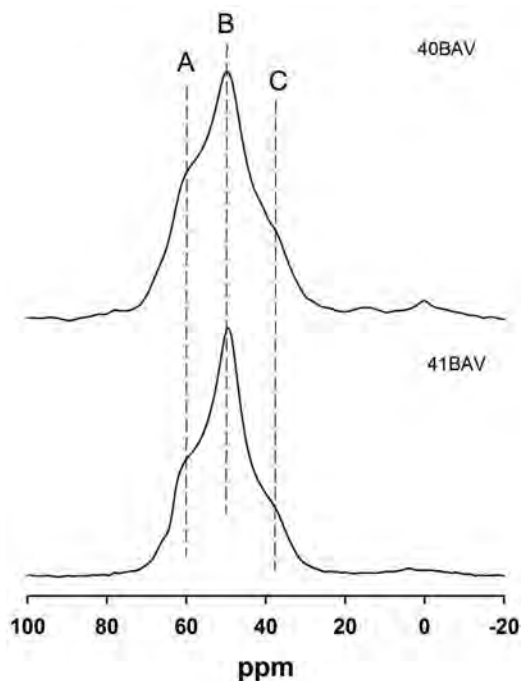


FIG. 11. ^{27}Al MAS NMR spectra for bavenites 40BAV and 41BAV; the three distinct bands are labelled A, B and C, and occur at 60, 51 and 38 ppm, respectively.

there is one maximum but the overall envelope also shows two distinct shoulders, three bands in all, labelled A, B and C in Fig. 11, indicating three distinct short-range arrangements around Al at $T(4)$. Thus the ^{27}Al MAS NMR spectra (Fig. 11) force us to conclude that $T(3)\text{Si}-\text{O}(3)-T(4)\text{Si}$ linkages are possible, and hence the arrangement $T(3)\text{Si}-T(4)\text{Si}-\text{Ca}-\square$ can occur. Moreover, the similarity in local incident bond-valence sums around O(3) for the arrangements $T(3)\text{Si}-T(4)\text{Si}-\text{Ca}-\square$ and $T(3)\text{Si}-T(4)\text{Al}-\text{Ca}-\text{H}$ suggests that the latter also can occur. Presumably there can be sufficient local relaxation of bondlengths to adjust to these arrangements.

FTIR spectroscopy

Fourier-transform infrared spectroscopy is sensitive to short-range order and has been used extensively to probe short-range order in complex solid-solutions (e.g. Hawthorne *et al.*, 1996b, 2000, 2005, 2007; Della Ventura *et al.*, 1996, 1998, 1999, 2007). Above, we argue that particular short-range arrangements should occur in bavenite. The FTIR spectra of four bavenite samples, 25BAV, 32BAV, 40BAV and 41BAV, are shown in Fig. 12. There are two principal maxima at ~ 3625 and $\sim 3545\text{ cm}^{-1}$. The envelope of the maximum at $\sim 3545\text{ cm}^{-1}$ has inflection points indicative of fine structure, and five sets of constituent bands (labelled A to E in Fig. 12) can be identified in the four spectra. There are two crystallographically

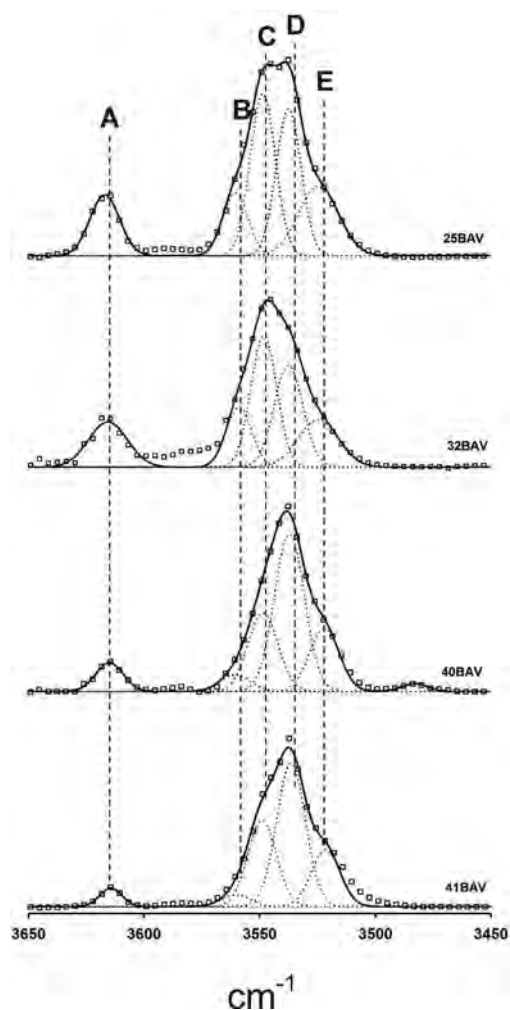


FIG. 12. FTIR spectra for selected bavenites in the principal (OH)-stretching region; data are shown as hollow squares.

distinct OH groups in the bavenite structure, O(8) (Fig. 6) and O(2) (Fig. 7), and the presence of more than two bands in the principal (OH)-stretching region is indicative of the presence of distinct short-range ordered arrangements around one or both of the O(8) and O(2) sites.

Above, we proposed one short-range arrangement around the O(8) site: $T^{(2)}\text{Be}-\text{Ca}-\text{Ca}-\text{O}(8)=\text{(OH)}$, and we expect one peak in the IR from this arrangement. For the O(2) site, only arrangements that involve (OH) at O(2) give signals in the IR, and there is one such nearest-neighbour arrangement: $T^{(3)}\text{Be}-\text{Ca}-\text{Ca}-\text{O}(2)=\text{(OH)}$. The O(3) anion bridges between the $T(3)$ and $T(4)$ tetrahedra and has four nearest-neighbour arrangements: $T^{(3)}\text{Si}-T^{(4)}\text{Si}$, $T^{(3)}\text{Si}-T^{(4)}\text{Al}$, $T^{(3)}\text{Be}-T^{(4)}\text{Si}$ and $T^{(3)}\text{Be}-T^{(4)}\text{Al}$. As a result, the bond valences incident at O(3) from these different nearest-neighbour arrangements will be different from each other, and the strengths of the resulting hydrogen bonds will be different, shifting the absorption frequency for each arrangement (and producing a concomitant relaxation around the O(2) anion as required by the valence-sum rule). Thus we expect four peaks in the IR from the arrangement $T^{(3)}\text{Be}-\text{Ca}-\text{Ca}-\text{O}(2)=\text{(OH)}$ due to the four next-nearest-neighbour arrangements around the acceptor O(3) anion in the adjacent $T(3)-T(4)-T(3)-T(4)$ ring: $T^{(3)}\text{Be}-T^{(4)}\text{Si}$ (arrangements 1 and 2, Table 10), $T^{(3)}\text{Be}-T^{(4)}\text{Al}$ (arrangement 3), $T^{(3)}\text{Si}-T^{(4)}\text{Al}$ (arrangements 5 and 6), and $T^{(3)}\text{Si}-T^{(4)}\text{Si}$ (arrangement 8). We now need to assign these arrangements to the bands fitted to the spectra in Fig. 12.

The cluster $T^{(2)}\text{Be}-\text{Ca}-\text{Ca}-\text{O}(8)=\text{(OH)}$ is present in the same amount in each sample, and shows no local variation around the H(8) atom that could give rise to fine structure, whereas the

TABLE 10. Scaled bond-valence sums at O(3) for all possible configurations from Table 9.

	$T(3)$	$T(4)$	Ca	H(2)	$T(3)-\text{O}(3)$	$T(4)-\text{O}(3)$	Ca-O(3)	H...O(3)	Σ (v.u.)	Possible
1	Be	Si	Ca	H	0.5	1.03	0.28	0.27	2.08	Yes
2	Be	Si	Ca	□	0.5	1.03	0.28	0	1.81	Yes
3	Be	Al	Ca	H	0.5	0.77	0.28	0.27	1.82	Yes
4	Be	Al	Ca	□	0.5	0.77	0.28	0	1.55	No
5	Si	Al	Ca	H	1.03	0.77	0.28	0.27	2.35	Yes
6	Si	Al	Ca	□	1.03	0.77	0.28	0	2.08	Yes
7	Si	Si	Ca	H	1.03	1.03	0.28	0.27	2.61	No
8	Si	Si	Ca	□	1.03	1.03	0.28	0	2.34	Yes

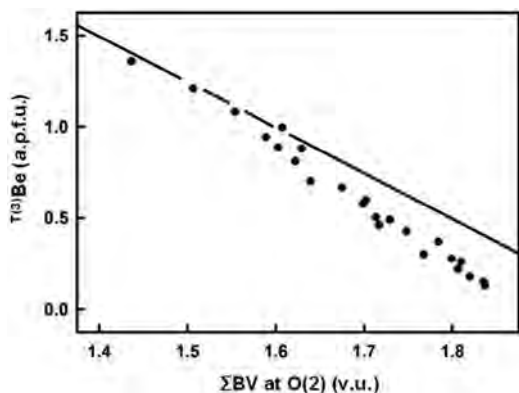


FIG. 13. Incident bond-valence at O(2) vs. ${}^{7(3)}\text{Be}$ a.p.f.u. for all bavenite samples. The ideal curve passes through 1.2 and 2.0 v.u. at the O(2) anion for ${}^{7(3)}\text{Be} = 2$ a.p.f.u. and unprotonated ${}^{7(3)}\text{Be} = 0$ a.p.f.u., respectively.

H(2) atom shows four different local arrangements of nearest- and next-nearest-neighbour cations that should give rise to four stretching bands in the infrared. The spectra (Fig. 12) show a single symmetrical band at $\sim 3635\text{ cm}^{-1}$ and a four-band envelope centred at $\sim 3545\text{ cm}^{-1}$. Accordingly, we assign the band at $\sim 3635\text{ cm}^{-1}$ (labelled A in Fig. 12) to the ${}^{7(2)}\text{Be}-\text{Ca}-\text{Ca}-\text{O}(8)=\text{(OH)}$ cluster and the envelope centred at $\sim 3545\text{ cm}^{-1}$ to bands involving the ${}^{7(3)}\text{Be}-\text{Ca}-\text{Ca}-\text{O}(2)=\text{(OH)}$ cluster (and labelled B–E in Fig. 12). Note that the amount of (OH) at the O(8) site (2 a.p.f.u., Table 3) is always in excess of the amount of (OH) at the O(2) site (< 2 a.p.f.u., Table 3) and yet the relative intensity of band A [assigned to (OH) at O(8)] is considerably less

than the relative intensity of the envelope of bands B–E assigned to (OH) at O(2) (Fig. 12). This is a result of the fact that the transition moment is an inverse function of the energy of the transition (where coupling of adjacent arrangements does not occur) (Skogby and Rossman, 1991; Burns and Hawthorne, 1994; Groat *et al.*, 1995).

Assignment of the B–E bands may be done by examining the relative strengths of the hydrogen bonds to O(3) required by the valence-sum rule. Where O(3) bridges the ${}^{7(3)}\text{Si}-{}^{7(4)}\text{Si}$ arrangement, the O(3) anion requires very little bond-valence from H(2), the associated O–H stretching frequency will be high, and band B may be assigned to this arrangement. Similarly, the bands C, D and E may be assigned to the local arrangements associated with increasing hydrogen-bond-valences: ${}^{7(3)}\text{Si}-{}^{7(4)}\text{Al}$, ${}^{7(3)}\text{Be}-{}^{7(4)}\text{Si}$ and ${}^{7(3)}\text{Be}-{}^{7(4)}\text{Al}$, respectively. This local effect has a strong influence on the long-range aspects of the structure around the O(2) site. This is shown by the variation in the calculated bond-valence sum at O(2) as a function of the (calculated) ${}^{7(3)}\text{Be}$ content for all samples (Fig. 13). Assuming an average $\text{O}_{\text{donor}}-\text{H}$ bond-valence of ~ 0.8 v.u., the incident bond-valence at O(2) should vary linearly between the points ($\Sigma\text{BVO}(2) = 2.0$, ${}^{7(3)}\text{Be} = 0.0$) where no H is present at O(2) and ($\Sigma\text{BVO}(2) = 1.2$, ${}^{7(3)}\text{Be} = 2.0$) where only (OH) is present at O(2). Although the data are broadly in accord with the model of SRO presented above, they do deviate systematically from the ideal relation (shown as the full line in Fig. 13). The data extrapolate to an incident bond-valence sum of ~ 1.9 v.u. for ${}^{7(3)}\text{Be} = 0.0$ a.p.f.u., indicating that the structure has significant strain

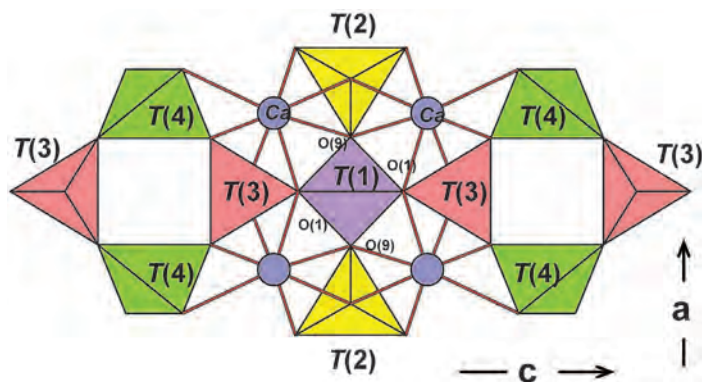


FIG. 14. The linkage of two $T(3)-T(4)-T(3)-T(4)$ rings along the c direction through the $T(1)$ tetrahedron projected onto (010); note that the $T(1)$ (= Si) tetrahedron links to two $T(2)$ (= Be) tetrahedra and two $T(3)$ (= Be and/or Si) tetrahedra.

around O(2) at this value, and that this local strain decreases with increasing Be and becomes zero at $T^{(3)}\text{Be} = 1.0$ a.p.f.u.

Short-range order controls the limits of $T^{(3)}\text{Be} \rightleftharpoons T^{(3)}\text{Si}$ substitution

As noted above, there are two end-members involved in the bavenite solid-solution series: $\text{Ca}_4\text{Be}_2\text{Si}_7\text{O}_{24}(\text{OH})_2[\text{Be}_2\text{Si}_2(\text{OH})_2]$ and $\text{Ca}_4\text{Be}_2\text{Si}_7\text{O}_{24}(\text{OH})_2[\text{Si}_2\text{Al}_2\text{O}_2]$. The compositions given here (Table 3, Fig. 8) span this range and do not extend much past the middle of the series toward the composition $\text{Ca}_4\text{Be}_2\text{Si}_7\text{O}_{24}(\text{OH})_2[\text{Be}_2\text{Si}_2(\text{OH})_2]$, in accord with the proposal of Beus (1966). What is the constraint that does not allow compositions in the second half of the compositional range?

The substitution $T^{(4)}\text{Si} + T^{(3)}\text{Be} + {}^{O(2)}\text{OH}^- \rightleftharpoons T^{(4)}\text{Al} + T^{(3)}\text{Si} + {}^{O(2)}\text{O}^{2-}$ involves the $T(3)$ and $T(4)$ tetrahedra. As shown in Fig. 1, these tetrahedra form a four-membered ring in the sequence $T(3)-T(4)-T(3)-T(4)$. Figure 14 shows the linkage of these rings in the c direction through the $T(1)$ (= Si) tetrahedron via the $T(3)$ tetrahedra of adjacent rings. Let us examine the short-range bond-valence distribution where one of the $T(3)$ tetrahedra is occupied by Be, and the other by a cation that gives a $T(3)-\text{O}(1)$ bond-valence of X v.u., taking the relevant values from Table 8. The sum of the bond valence incident at the $T(1)$ tetrahedron is as follows: $0.44 \times 2 [T(2)-\text{O}(9) \times 2] + 0.27 \times 4 [Ca-\text{O}(9) \times 4] + 0.41 \times 1 [T(3)-\text{O}(1), T(3) = \text{Be}] + 0.21 \times 4 [Ca-\text{O}(1) \times 4] + X [T(3)-\text{O}(1), T(3) = \text{not specified}] = (3.21 + X)$ v.u. As $T(1) = \text{Si}$, the valence-sum rule requires that the bond-valence incident at the $T(1)$ tetrahedron is 4 v.u., and hence $X = 0.79$ v.u. Inspection of the local bond-valence arrangement where $T(3) = \text{Si}$ (Table 8*b*) shows that $T(3)-\text{O}(1)$ has a bond valence of 0.82 v.u., close to the value of 0.79 v.u. required for satisfaction of the bond-valence requirements of the $T(1)$ tetrahedron where $T(1)$ links to Be at one of the two adjacent $T(3)$ sites. Thus, where $T^{(3)}\text{Be}$ participates in the linkage $T(3)-T(1)-T(3)$, the local arrangement $T^{(3)}\text{Be}-T^{(1)}\text{Si}-T^{(3)}\text{Si}$ is forced by the bond-valence requirements of the $T(1)$ tetrahedron. Hence $T^{(3)}\text{Be}$ cannot exceed $T^{(3)}\text{Si}$ in the substitution $T^{(4)}\text{Si} + T^{(3)}\text{Be} + {}^{O(2)}\text{OH}^- \rightleftharpoons T^{(4)}\text{Al} + T^{(3)}\text{Si} + {}^{O(2)}\text{O}^{2-}$, accounting for a range in substitution from $\text{Ca}_4\text{Be}_2\text{Si}_7\text{O}_{24}(\text{OH})_2[\text{Si}_2\text{Al}_2\text{O}_2]$ to $\text{Ca}_4\text{Be}_2\text{Si}_7\text{O}_{24}(\text{OH})_2[\text{BeAlSi}_2(\text{OH})\text{O}]$ (Beus, 1966) and the lack of

compositions between $\text{Ca}_4\text{Be}_2\text{Si}_7\text{O}_{24}(\text{OH})_2[\text{BeAlSi}_2(\text{OH})\text{O}]$ and $\text{Ca}_4\text{Be}_2\text{Si}_7\text{O}_{24}(\text{OH})_2[\text{Be}_2\text{Si}_2(\text{OH})_2]$.

The role of Na in promoting 'excess' Be in the structure of bavenite

Inspection of Table 3 and Fig. 8 shows that Be does exceed 3.0 a.p.f.u. in bavenite, in apparent contradiction to the above argument that $\text{Be} \rightleftharpoons \text{Si}$ substitution is limited by local bond-valence requirements at the $T(1)$ tetrahedron. However,

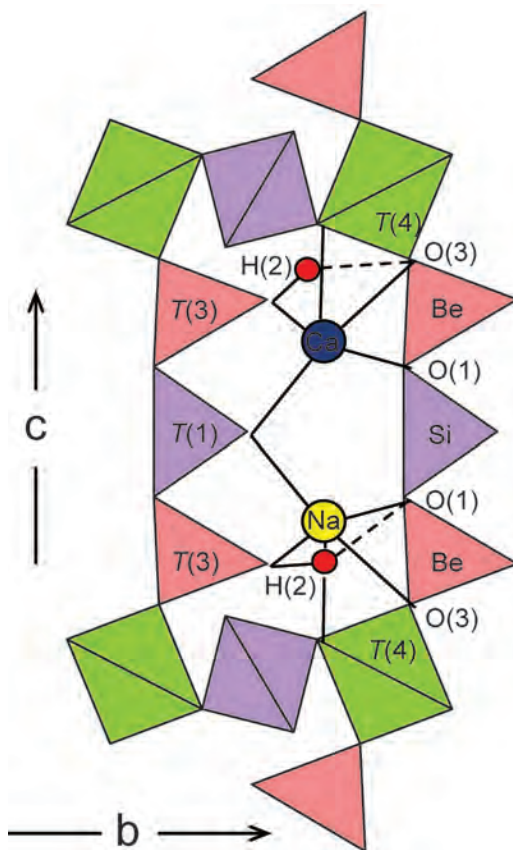
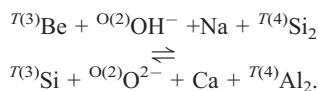


FIG. 15. The linkage of two $T(3)-T(4)-T(3)-T(4)$ rings along the c direction through the $T(1)$ tetrahedron projected onto (100); in the upper part of the figure, the Ca site is occupied by Ca (blue), whereas in the lower part of the figure, the Ca site is occupied by Na (yellow). Note that $H(2)$ forms a hydrogen bond with $O(1)$ where locally associated with Na at the Ca site, and the adjacent $T(3)$ site is occupied by Be , forming a $T^{(3)}\text{Be}-T^{(1)}\text{Si}-T^{(3)}\text{Be}$ link.

Fig. 9 shows that this ‘excess’ Be is accompanied by replacement of Ca by Na. This is a rather unusual substitution as both substituents (Na, Be) must replace cations of higher formal charge. In order to maintain electroneutrality, either there must be replacement of Si by Al by the amount (Na + excess Be) or replacement of O by (OH). The above argument that incorporation of Be at $T(3)$ must be accompanied by incorporation of (OH) at O(2) still holds, and hence the substitution is thus



Although the amounts involved are small, this substitution is also indicated by the fact that the two Be-rich (and Na-rich) points in Fig. 5 (corresponding to 12BAV and 35BAV) lie below the 1:1 line between $T(4)\text{Al}$ and $T(3)\text{Be}$. This second substitution is similar to the first, with the addition of $\text{Na} + T(4)\text{Si} \rightleftharpoons \text{Ca} + T(4)\text{Al}$; as none of these constituents is Be, one needs to ask (1) what is the role of Na in this substitution, and (2) how does the incorporation of Na negate the linkage constraint (in the *c* direction) on the amount of Be in the structure?

Figure 15 shows the local arrangement around the $T(3)$ – $T(1)$ – $T(3)$ linkage in the *c* direction. The upper H(2) hydrogen shows the usual hydrogen-bond to the O(3) anion where $T(3)$ is occupied by Be. In Fig. 15, the $T(3)$ tetrahedron (top right,

labelled Be) links to a $T(1)$ tetrahedron (labelled Si) as shown (horizontally) in Fig. 14. This $T(1)$ tetrahedron then links (shown in Fig. 15) to a $T(3)$ tetrahedron of another $T(3)$ – $T(4)$ – $T(3)$ – $T(4)$ ring, and the lower $T(3)$ tetrahedron is commonly constrained to be occupied by Si (as discussed above). However, if the *Ca* site is actually occupied by Na (Fig. 15, bottom), the adjacent H(2) is not as strongly repelled from Na as from Ca, and can form a hydrogen bond with the adjacent O(1) anion as shown at the bottom of Fig. 15. This arrangement will provide more bond valence to O(1) which is normally the case where the *Ca* site is occupied by Ca. Is it enough to materially effect the occupancy of the adjacent $T(3)$ site? As discussed above, the bond-valence incident at the linking $T(1)$ tetrahedron is $0.44 \times 2 [T(2)\text{–O}(9) \times 2] + 0.27 \times 4 [Ca\text{–O}(9) \times 4] + 0.41 \times 1 [T(3)\text{–O}(1), T(3) = \text{Be}] + 0.21 \times 4 [Ca\text{–O}(1) \times 4] + X [T(3)\text{–O}(1), T(3) = \text{not specified}] = (3.21 + X)$ v.u. where *X* is the bond valence supplied by the other $T(3)$ site involved in the $T(3)$ – $T(1)$ – $T(3)$ linkage in the *c* direction. For the local arrangement where the *Ca* site is occupied by Na (Fig. 15, top), this value of $(3.21 + X)$ v.u. is modified by subtracting the value for one Ca–O(1) bond (0.21 v.u., Table 8a), replacing it by the bond valence from the analogous Na–O(1) bond (0.18 v.u.), and adding the contribution from the hydrogen bond (0.27 v.u., Table 8a), leading to a bond-valence incident at the linking $T(1)$ tetrahedron of $(3.21 - 0.21 + 0.18$

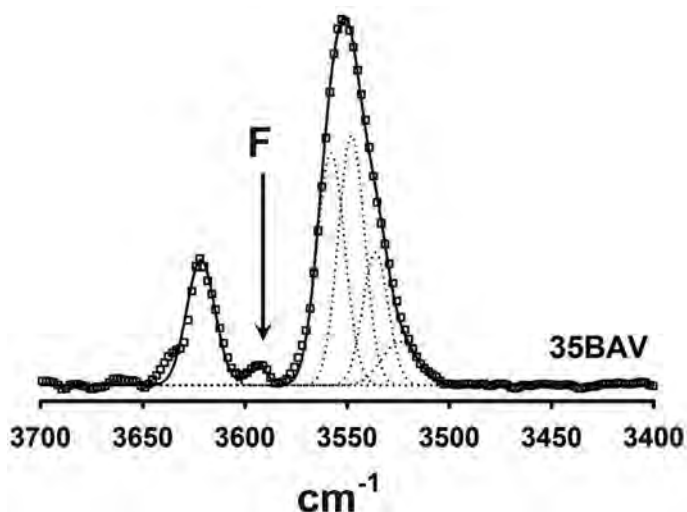


FIG. 16. The FTIR spectrum for Na-bearing bavenite BAV35 in the principal OH-stretching region; data are shown as hollow squares.

+ 0.27 + X) = 3.45 v.u.: X = 0.55 v.u. This value is significantly closer to the short-range Be–O(1) value of 0.41 v.u. than the corresponding Si–O(1) value of 0.81 v.u. (Table 8a,b), indicating that Be can occupy the second $T(3)$ tetrahedron in the $T(3)$ – $T(1)$ – $T(3)$ linkage in the c direction where the adjacent Ca site is occupied by Na instead of Ca. The difference between the Be–O(1) values of 0.41 and 0.55 v.u., and the close approach of the H(2) and Na atoms probably make this a highly strained arrangement, but it is clear from the compositions observed for 12BAV and 35BAV that this arrangement can occur in small amounts. However, such strain obviously limits the amount of this substitution, accounting for the rarity of bavenite compositions with Be >3 a.p.f.u.

The change in hydrogen bonding in the Na-bearing structure is visible in the IR. Figure 16 shows the IR spectrum of bavenite 35BAV with 0.145 Na a.p.f.u. In addition to the five bands that are present in all the other bavenite spectra recorded (Fig. 12), there is a band at $\sim 3590\text{ cm}^{-1}$ that is not present in the other spectra. We assign this to the proposed H(2)...O(1) hydrogen bond associated with the incorporation of Na into the bavenite structure.

Acknowledgements

The authors are grateful to all those who donated and provided samples for study: Excaliber Mineral Co., Harvard University, Royal Ontario Museum (Toronto), Natural History Museum (Vienna), Petr Černý (University of Manitoba), Moravia Museum of Mineralogy, Geologisk Museum (Copenhagen), Andy McDonald (Laurentian University). We thank Mark Cooper for his help with the experimental work. This work was funded by a Canada Research Chair in Crystallography and Mineralogy, NSERC Discovery and Research Tools and Equipment Grants to FCH, an NSERC PGS-D and a University of Manitoba Graduate Fellowship Award to AJL, and Canada Foundation for Innovation grants to FCH.

References

- Berry, L.G. (1963) The composition of bavenite. *American Mineralogist*, **48**, 1166–1168.
- Beus, A.A. (1966) *Geochemistry of Beryllium and Genetic Types of Beryllium Formations*. Izd-vo Akademii Nauk, SSSR, Moscow (in Russian).
- Bondi, M., Griffin, W.L., Mattioli, V. and Mottana, A. (1983) Chiavennite, $\text{CaMnBe}_2\text{Si}_5\text{O}_{13}(\text{OH})_2 \cdot 2\text{H}_2\text{O}$, a new mineral from Chiavenna (Italy). *American Mineralogist*, **68**, 623–627.
- Brown, G.E. and Gibbs, G.V. (1969) Oxygen coordination and the Si–O bond. *American Mineralogist*, **54**, 1528–1539.
- Brown, I.D. (2002) *The Chemical Bond in Inorganic Chemistry: The Bond-Valence Model*. Oxford University Press, Oxford, UK.
- Brown, I.D. and Altermatt, D. (1985) Bond-valence parameters obtained from a systematic analysis of the inorganic crystal structure database. *Acta Crystallographica*, **B41**, 244–247.
- Burns, P.C. and Hawthorne, F.C. (1994) Structure and hydrogen bonding in preobrazhenskite, a complex heteropolyhedral borate. *The Canadian Mineralogist*, **32**, 387–396.
- Cannillo, E., Coda, A. and Fagani, G. (1966) The crystal structure of bavenite. *Acta Crystallographica*, **20**, 301–309.
- Černý, P. (1968) Alteration of beryl in pegmatites; the process and its products. *Neues Jahrbuch für Mineralogie Abhandlungen*, **108**, 166–180.
- Černý, P. (2002) Mineralogy of beryllium in granitic pegmatites. Pp. 405–444 in: *Beryllium: Mineralogy, Petrology, and Geochemistry* (E.S. Grew, editor). Reviews in Mineralogy and Geochemistry, **50**, Mineralogical Society of America and Geochemical Society, Washington, D.C.
- Della Ventura, G., Robert, J.-L., Hawthorne, F.C. and Prost, R. (1996) Short-range disorder of Si and Ti in the tetrahedral double-chain unit of synthetic Ti-bearing potassium-rich richterite. *American Mineralogist*, **81**, 56–60.
- Della Ventura, G., Robert, J.-L. and Hawthorne, F.C. (1998) Characterization of OH-F short-range order in potassium-fluor-rich richterite by infrared spectroscopy in the OH-stretching region. *The Canadian Mineralogist*, **36**, 181–185.
- Della Ventura, G., Hawthorne, F.C., Robert, J.-L., Delbove, F., Welch, M.F. and Raudsepp, M. (1999) Short-range order of cations in synthetic amphiboles along the richterite-pargasite join. *European Journal of Mineralogy*, **11**, 79–94.
- Della Ventura, G., Oberti, R., Hawthorne, F.C. and Bellatreccia, F. (2007) FTIR spectroscopy of Ti-rich pargasites from Lherz and the detection of O^{2-} at the anionic O3 site in amphiboles. *American Mineralogist*, **92**, 1645–1651.
- Groat, L.A., Hawthorne, F.C. and Rossman, G.R. (1995) The infrared spectroscopy of vesuvianite in the OH region. *The Canadian Mineralogist*, **33**, 609–626.
- Hawthorne, F.C. (1997) Short-range order in amphiboles: a bond-valence approach. *The Canadian Mineralogist*, **35**, 201–216.
- Hawthorne, F.C. and Della Ventura, G. (2007) Short-

- range order in amphiboles. Pp. 173–222 in: *Amphiboles: Crystal Chemistry, Occurrence and Health Issues* (F.C. Hawthorne, R. Oberti, G. Della Ventura and A. Mottana, editors). Reviews in Mineralogy and Geochemistry, **67**, Mineralogical Society of America and Geochemical Society, Washington, D.C.
- Hawthorne, F.C. and Grice, J.D. (1990) Crystal structure analysis as a chemical analytical method: application to light elements. *The Canadian Mineralogist*, **28**, 693–702.
- Hawthorne, F.C. and Huminicki, D.M.C. (2002) The crystal chemistry of beryllium. Pp. 333–403 in: *Beryllium: Mineralogy, Petrology, and Geochemistry* (E.S. Grew, editor). Reviews in Mineralogy and Geochemistry, **50**, Mineralogical Society of America and Geochemical Society, Washington, D.C.
- Hawthorne, F.C., Ungaretti, L. and Oberti, R. (1995) Site populations in minerals: terminology and presentation of results of crystal-structure refinement. *The Canadian Mineralogist*, **33**, 907–911.
- Hawthorne, F.C., Oberti, R. and Sardone, N. (1996a) Sodium at the A site in clin amphiboles: the effects of composition on patterns of order. *The Canadian Mineralogist*, **34**, 577–593.
- Hawthorne, F.C., Della Ventura, G. and Robert, J.-L. (1996b) Short-range order of (Na,K) and Al in tremolite: An infrared study. *American Mineralogist*, **81**, 782–784.
- Hawthorne, F.C., Welch, M.D., Della Ventura, G., Liu, S., Robert, J.-L. and Jenkins, D.M. (2000) Short-range order in synthetic aluminous tremolites: An infrared and triple-quantum MAS NMR study. *American Mineralogist*, **85**, 1716–1724.
- Hawthorne, F.C., Della Ventura, G., Oberti, R., Robert, J.-L. and Iezzi, G. (2005) Short-range order in minerals: amphiboles. *The Canadian Mineralogist*, **43**, 1895–1920.
- Hawthorne, F.C., Oberti, R. and Martin, R.F. (2006) Short-range order in amphiboles from the Bear Lake diggings, Ontario. *The Canadian Mineralogist*, **44**, 1171–1179.
- Janeczek, J. (1985) Typomorphism of pegmatite minerals in the Strzegom-Sobotka granite massif. *Geologia Sudetica*, **20**, 1–68 (in Polish).
- Kharitonov, Yu.A., Kuz'min, E.A., Ilyukhin, V.V. and Belov, N.V. (1971) The crystal structure of bavenite. *Journal of Structural Chemistry*, **12**, 72–76.
- Peterson, O.V., Micheelsen, H.I. and Leonardsen, E.S. (1995) Bavenite, $\text{Ca}_4\text{Be}_3\text{Al}[\text{Si}_9\text{O}_{25}(\text{OH})_3]$, from the Ilimaussaq alkaline complex, South Greenland. *Neues Jahrbuch für Mineralogie Monatshefte*, **21**, 321–335.
- Shannon, R.D. (1976) Revised effective ionic radii and systematic studies of interatomic distances in halides and chalcogenides. *Acta Crystallographica*, **A32**, 751–757.
- Skogby, H. and Rossman, G.R. (1991) The intensity of amphibole OH bands in the infrared absorption spectrum. *Physics and Chemistry of Minerals*, **1**, 64–68.
- Switzer, G. and Reichen, L.E. (1960) Re-examination of pilinite and its identification with bavenite. *American Mineralogist*, **45**, 757–762.
- Tennyson, C. (1960) Berylliummineralien und ihre pegmatitische Paragenese in den Graniten von Tittling/Bayerischer Wald. *Neues Jahrbuch für Mineralogie Abhandlungen*, **94**, 1253–1265.